Title
A NUMERICAL STUDY OF KELVIN-HELMBOLTZ INSTABILITY BY THE POINT VORTEX METHOD

Author
Krasny, R.

Publication Date
1983-12-01

Lawrence Berkeley Laboratory
UNIVERSITY OF CALIFORNIA

Physics Division

Mathematics Department

A NUMERICAL STUDY OF KELVIN-HELMHOLTZ INSTABILITY
BY THE POINT VORTEX METHOD

R. Krasny
(Ph.D. Thesis)

December 1983

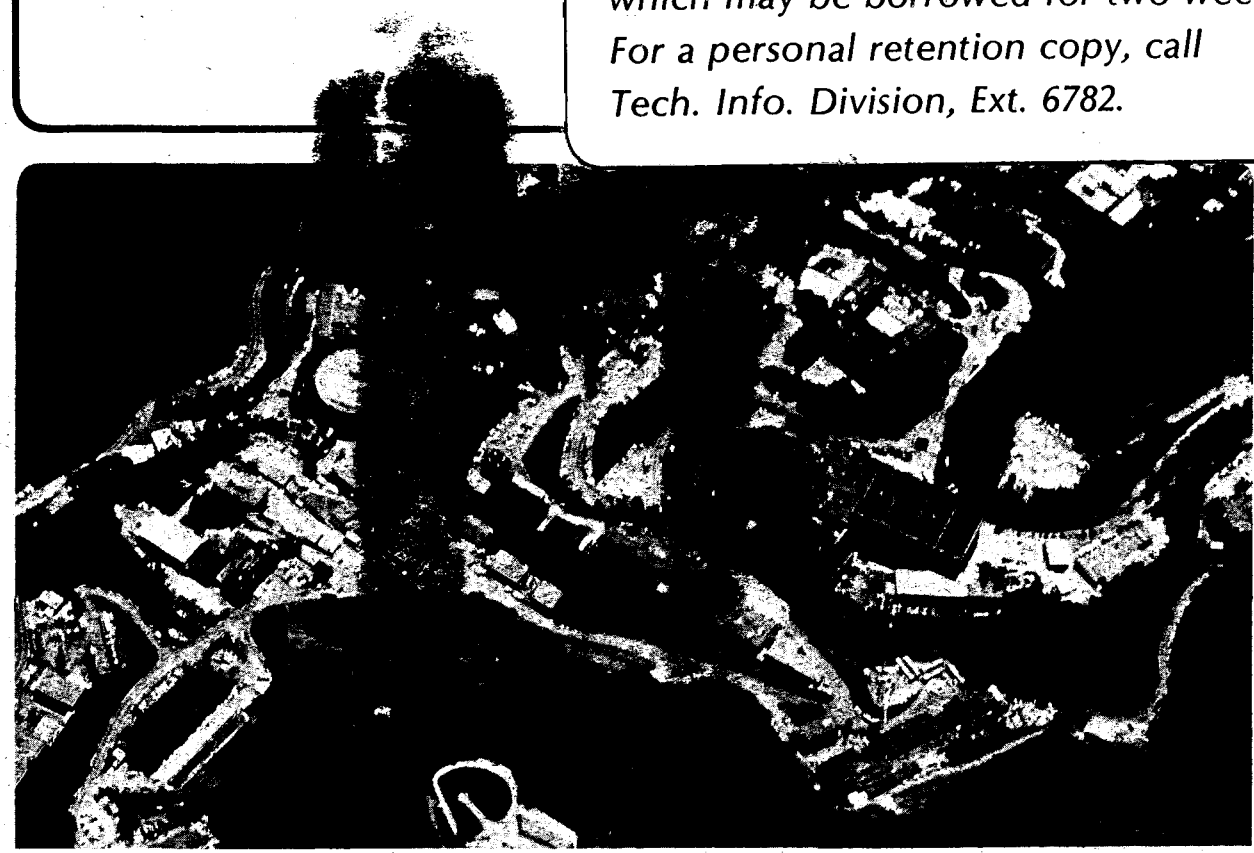

Prepared for the U.S. Department of Energy under Contract DE-AC03-76SF00098

DISCLAIMER

LBL-17092

A NUMERICAL STUDY OF KELVIN-HELMHOLTZ INSTABILITY BY THE POINT VORTEX METHOD[1]

Robert Krasny

Lawrence Berkeley Laboratory
and
Department of Mathematics
University of California
Berkeley, California 94720

Ph.D. Thesis

December 1983

[1]This work was supported in part by the Director, Office of Energy Research, Office of Basic Energy Sciences, Engineering, Mathematical, and Geosciences Division of the U.S. Department of Energy under contract DE-AC03-76SF00098.

A Numerical Study of Kelvin-Helmholtz Instability by the Point Vortex Method

Robert Krasny

Abstract

Rosenhead's classical point vortex numerical method for studying the evolution of a vortex sheet from analytic initial data (Kelvin-Helmholtz instability) is examined using the discrete Fourier analysis techniques of Sulem, Sulem & Frisch. One cause for the "chaotic" motion previously observed in computations using a large number of vortices is that short wavelength perturbations are introduced spuriously by finite precision arithmetic and become amplified by the model's dynamics. Methods for controlling this source of error are given and the results confirm the formation of a singularity in a finite time which was previously found by Moore and Meiron, Baker & Orszag using different techniques of analysis. A cusp forms in the vortex sheet strength at the critical time, explaining the onset of erratic particle motion in applications of the numerical methods of Van de Vooren and Fink & Soh to this problem. Unlike those methods, the point vortex approximation remains consistent at the critical time and we present the results of a long time calculation. The singularity is interpreted physically as a discontinuity in the strain rate along the vortex sheet and also as the start of roll up on a small scale. We numerically study some aspects of the dependence of the solution on the initial condition and find agreement with Moore's asymptotic relation between the initial amplitude and the critical time. For large initial amplitudes, two cusps form in the sheet strength, corresponding to double roll up. We explain why the Poincaré recurrence theorem does not imply that the sheet will eventually unroll. Our results suggest that

beyond the critical time, the vortex sheet becomes a spiral with infinite arclength although we have doubts about the approximation's accuracy in that regime.

Acknowledgements

It is with pleasure that I thank my thesis advisor, Alexandre Chorin, for his enthusiastic interest in my research. I am also grateful for having received inspiration, instruction and encouragement from him during my graduate studies at Berkeley.

I wish to thank Ole Hald for the detailed comments he made on an early version of this manuscript. I also appreciate having been exposed, as a student in his classes and as a teaching assistant under his supervision, to the example he set of commitment to high standards.

I thank Antoni Oppenheim for serving as my thesis committee's outside member.

I am happy to express my gratitude to Gilles Corcos for generously sharing his physical insight with me during our discussions and for his helpful comments throughout my thesis research. I have also benefited from the penetrating remarks made by Edward Fraenkel who kindly agreed to read my manuscript.

I take this opportunity to thank Ray Chin for introducing me to the research process early in my graduate studies.

I thank Paul Concus and the Department of Computer Science and Mathematics, Lawrence Berkeley Laboratory, for the support I have received as a Graduate Student Research Assistant and for making available to me their fine computing resources. I thank the University of California for having awarded me a Regents Fellowship.

I wish to thank my fellow students and friends, Chris Anderson, Claude Greengard and Mirta Perlman with whom I have had many enjoyable conversations. Above all, I thank my mother and father and my brother, Jerrold.

CONTENTS

0. Introduction

In this paper we study the vortex sheet model for the instability of a parallel shear flow. We consider the nonlinear temporal instability to analytic perturbations of the following weak solution, with shear, of the Euler equations:

$$u(x,y) = \begin{cases} -U & \text{if } y>0\,, \\ U & \text{if } y<0\,, \end{cases} \qquad v(x,y) = 0\,, \tag{0.1}$$

where (u,v) are the Cartesian components of the velocity and U is a positive constant. The effects of density stratification, compressibility, body forces, surface tension, viscosity, boundaries and three dimensionality will be ignored.

The interface separating the two fluid regions is a vortex sheet and the classical point of view (Prandtl & Tietjens 1934), based on experimental observation, was that a sinusoidally perturbed sheet rolls up smoothly into local concentrations of vorticity as in figure 0.1 . A vortex sheet can be described by a curve in the complex plane:

$$Z(\Gamma,t) = X(\Gamma,t) + iY(\Gamma,t)\,,$$

where t is time and Γ is a Lagrangian parameter which measures the circulation between a base point $\Gamma=0$ and an arbitrary point along the sheet (Birkhoff 1962). The vortex sheet strength $\sigma(\Gamma,t)$ is the tangential jump in velocity across the sheet and is determined up to sign by:

$$\sigma(\Gamma,t) = |\,Z_\Gamma\,|^{-1} \quad , \quad Z_\Gamma = \frac{\partial Z}{\partial \Gamma}\,.$$

Consider a vortex sheet for which $Z(\Gamma,t) - \Gamma/2U$ is periodic in Γ with period $2U\lambda$. It follows that $Z(\Gamma+2U\lambda,t) = Z(\Gamma,t) + \lambda$ so that λ is the wavelength in the x direction. Define dimensionless variables (primed) by:

$$\Gamma = 2U\lambda\Gamma' \quad , \quad t = 2Ut'/\lambda \quad , \quad Z = \lambda Z' \ .$$

The initial value problem for the vortex sheet in nondimensional form (dropping the primes) is:

$$\frac{\partial \overline{Z}}{\partial t}(\Gamma, t) = \frac{1}{2i} \not\int_0^1 \cot\pi(Z(\Gamma, t) - Z(\tilde{\Gamma}, t)) \, d\tilde{\Gamma} \ , \tag{0.2a}$$

$$Z(\Gamma, 0) = \Gamma + P(\Gamma, 0) \ . \tag{0.2b}$$

The bar on the left side of (0.2a) denotes complex conjugate and the slash on the integral sign denotes a Cauchy principal value.

Equation (0.2a) , the kinematical condition that the vortex sheet be a free surface, is a special case of the Biot-Savart law relating vorticity and velocity in incompressible flow. The dynamical requirement that circulation around material curves be preserved is implicitly contained in the understanding that Γ is a Lagrangian variable. The vortex sheet may be written as the sum:

$$Z(\Gamma, t) = \Gamma + P(\Gamma, t) \ ,$$

where $P(\Gamma, t)$ is a periodic perturbation of the flat, constant strength vortex sheet corresponding to the equilibrium flow (0.1). For each wavenumber k, the linearized problem admits two solutions having exponential growth and decay rates kU, the well known linear Kelvin-Helmholtz instability (Batchelor 1968). These linear modes are given nondimensionally by :

$$Z(\Gamma, t) = \Gamma + \alpha \, e^{2\pi t}(1 - i) \sin 2\pi\Gamma \ , \tag{0.3a}$$

$$Z(\Gamma, t) = \Gamma + \alpha \, e^{-2\pi t}(1 + i) \sin 2\pi\Gamma \ , \tag{0.3b}$$

and are displayed in figure 0.2 . In this paper, the initial perturbation $P(\Gamma, 0)$ will be a linear combination of at most two such linear theory modes of small amplitude. In particular, the initial perturbations will be analytic functions, a crucial assumption for the viability of the vortex sheet model.

Birkhoff (1962) conjectured that a solution of equations (0.2) which is initially analytic remains so for at least a finite time. A proof of this conjecture has recently been advanced by Sulem, Sulem, Bardos & Frisch (1981). Noting that linear theory predicts faster growth rates for shorter wavelength perturbations and assuming that nonlinear interactions will perturb all wavelengths, one may suspect that a singularity forms in a finite time even for analytic initial data. Indeed, Birkhoff conjectured that this would occur in the absence of surface tension and viscosity. Moore (1979) performed an asymptotic analysis which suggested that a curvature singularity does form at a critical time which depends upon the initial perturbation amplitude. Using Taylor series in time Meiron, Baker & Orszag (1982) have obtained numerical results in agreement with Moore's asymptotics. They found that at the critical time the vortex sheet strength has a cusp although the interface is only slightly distorted and possesses none of the features associated with roll up (as previously noted by Moore). Both Moore and Meiron, Baker & Orszag viewed the formation of this singularity as a possible restriction on the validity of the vortex sheet model.

With these recent papers there is emerging a consistent picture of the nonlinear Kelvin-Helmholtz instability. This contrasts with the confusion aroused by the failure of standard numerical methods to solve equations reliably (0.2). We will now briefly survey the large literature on these methods; see also Pullin (1982), Moore (1981) and Saffman & Baker (1979).

The classical approach to the numerical solution of (0.2), introduced by Rosenhead (1931), is to replace the curve $Z(\Gamma, t)$ at a fixed time by a finite number of particles corresponding to a uniform Γ-mesh. Thus $\{Z_j(t) ; j=1, \ldots, N\}$ approximates $\{Z(\Gamma_j, t) ; j=1, \ldots, N\}$ where $\Gamma_j = (j-1)\Delta\Gamma$, $N\Delta\Gamma = 1$ and N is the number of particles per wavelength. The integral on the right side of (0.2a) is approximated by trapezoidal quadra-

ture and the infinite contribution due to the integrand's singularity is ignored. This gives a system of ordinary differential equations for the particle paths:

$$\frac{d\bar{Z}_j}{dt} = \frac{1}{2iN} \sum_{\substack{k=1 \\ k \neq j}}^{N} \cot \pi (Z_j - Z_k) , \tag{0.4a}$$

$$Z_j(0) = \Gamma_j + P(\Gamma_j, 0) . \tag{0.4b}$$

Equation (0.4a) also describes the evolution of N periodic rows of equal strength point vortices. In this interpretation the omission $k \neq j$ corresponds to the fact that a point vortex (and more generally a periodic row of point vortices) has zero self induced velocity. The dynamical requirement that the strength of each point vortex does not change in time is implicit. A related fact, implicit in the discretization of $Z(\Gamma, t)$, is that the point vortices are ordered by continuity in Γ. This ordering doesn't change in time and allows the points to be connected by a curve which approximates the exact interface.

We remark that a discrete system of equal strength point vortices, equally spaced on a straight line, is linearly unstable in a fashion which closely mimics the linear Kelvin-Helmholtz instability of a continuous vortex sheet (Lamb 1932). The fastest growing mode of this discrete linear instability is an interaction between pairs of adjacent vortices.

For future reference, we record that the point vortex equations (0.4) form a finite dimensional Hamiltonian system with Hamiltonian:

$$H_N(t) = \frac{-1}{2\pi N^2} \sum_{j=1}^{N} \sum_{\substack{k=1 \\ k \neq j}}^{N} \ln \left| \sin \pi (Z_j(t) - Z_k(t)) \right| . \tag{0.5}$$

The continuous system (0.2) has an analogous conserved quantity (Van de Vooren 1965, pub. 1980):

$$H(t) = \frac{-1}{2\pi}\int_0^1\int_0^1 \ln \mid \sin\pi(Z(\Gamma,t)-Z(\tilde{\Gamma},t)) \mid d\Gamma d\tilde{\Gamma}. \qquad (0.6)$$

Rosenhead integrated the real and imaginary parts of (0.4) by Euler's method. The initial condition was a transverse sinusoidal perturbation of the flat constant strength vortex sheet. A copy of these calculations, performed on desk machines with $N = 12$, is shown in figure 0.3 . The interpolating curve that was drawn through the point vortices indicates a smooth roll up.

These calculations were accepted as support for Prandtl's conception of Kelvin-Helmholtz instability until challenged by Birkhoff (1962). He viewed Rosenhead's work as inconclusive since convergence of the method had not been demonstrated. Birkhoff also gave the following reasons for doubting the validity of Prandtl's speculations:

(1) the greater instability of perturbations of short wavelength,

(2) the reversibility and (presumed) asymptotic tendency towards randomness of conservative dynamical systems.

These doubts were reinforced by computer calculations (Birkhoff & Fisher (1959)) using N=20 and fourth order Runge-Kutta time integration. Some of these results are reproduced in figure 0.4 . In all cases the evolution eventually exhibited irregular and apparently random motion of the point vortices. Birkhoff discounted the effect of truncation and roundoff errors and concluded that the smooth roll up observed physically depends on the influence of viscosity.

Since then, Rosenhead's method has fallen into disrepute. Investigators have focussed on repairing the presumed defect in the point vortex approximation, namely the fact that close to a point vortex the induced singular velocity field poorly approximates the tangential velocity jump of a vortex sheet. Two general approaches to this issue have emerged:

(1) an analytic approach which seeks to account for the velocity contribution of the portion of the sheet neglected in (0.4a),

(2) a vortex blob approach in which the singular velocity field is smoothed by convolution with a cutoff function.

In the analytic approach, advanced by Van de Vooren (1965, pub. 1980), the Cauchy principal value integral in (0.2a) is replaced by an equivalent integral whose integrand has a removable singularity. The trapezoidal rule is then applied yielding a system of equations which differs from (0.4a) only in the addition of a correction term to the right side:

$$\frac{d\bar{Z}_j}{dt} = \frac{1}{2iN}\sum_{\substack{k=1 \\ k\neq j}}^{N} \cot \pi(Z_j - Z_k) + \frac{1}{4\pi iN}\left[\frac{Z_{\Gamma\Gamma}}{Z_\Gamma^2}\right]_j , \qquad (0.7)$$

where the last term is evaluated at Γ_j (Moore 1981). Van de Vooren used a numerical differentiation rule exact for eighth degree polynomials to approximate these derivatives. Calculations using $N = 40, 80$ led to irregularities sooner in some cases than with the uncorrected equation (0.4a). Van de Vooren attributed this to instability and roundoff error although no evidence was presented to support such claims. A pseudospectral method for calculating Z_Γ and $Z_{\Gamma\Gamma}$, proposed by Conte & Sherman (1979), also led to irregularities.

Other work in this vein was done by Fink & Soh (1978), Baker (1979), Pullin (1982), and Bromilow & Clements (1983) among others. One trend has been to include physical effects which stabilize aspects of the linear problem (e.g. stable density stratification and surface tension (Chandresekhar 1965)). Different numerical techniques have been tried (predictor-corrector ODE solvers, numerical differentiation of interpolating splines, resetting the particles at each time step to be equidistant in chordlength, ad-hoc numerical smoothing). While acheiving success in a variety of flow situations these

methods have all run aground on Kelvin-Helmholtz instability. For the related problem of Rayleigh-Taylor instability, it has been noted that using large numbers of computational elements causes the computation's reliability to deteriorate (Baker, Meiron & Orszag 1980).

Moore (1981) has shown that, for point vortex approximation of a circular vortex sheet of constant strength, chaotic motion is caused by growth of numerical errors due to linear Kelvin-Helmholtz instability. He demonstrated that the onset of this chaotic motion could be delayed by the linear smoothing formula of Longuet-Higgins & Cokelet (1976) and by the repositioning technique of Fink & Soh (1978). Moore also advocated abandoning the vortex sheet model in favor of a vortex layer of finite thickness for which short wavelength perturbations are linearly stable.

Chorin & Bernard (1973) introduced the vortex blob method to study the vortex sheet shed by an elliptically loaded wing. Later work using vortex blobs has concentrated on boundary layers and smooth vorticity distributions with little direct relation to the instability of a free vortex sheet (Chorin (1978), Hald (1979), Beale & Majda (1982)). Acton (1976), Ashurst (1979) and Nakamurma, Leonard & Spalart (1982) have used the blob method to study vortex layers of finite thickness and Anderson (1983) has extended the blob method to treat the roll up of an interface separating fluids of different densities. To my knowledge, no vortex blob calculations for a periodically perturbed vortex sheet have been published.

The aim of this paper is to resolve some of the issues surrounding previous numerical studies of Kelvin-Helmholtz instability with analytic initial perturbations. We will use discrete Fourier analysis to examine results computed by Rosenhead's point vortex approximation. Our numerical experiments show that the irregular vortex motion previously observed has several distinct causes:

(1) amplification, due to linear Kelvin-Helmholtz instability, of shortwave perturbations introduced by roundoff error,

(2) improper balance between time and spatial truncation errors,

(3) loss of analyticity in finite time which causes the correction term in (0.7) to become undefined,

(4) misinterpretation of numerical results for certain initial conditions.

The first phenomenon is an effect of the computer's finite precision arithmetic and may be abated by methods discussed in section 1. High resolution results (N=100) far into the nonlinear regime are presented which show a smooth roll up similar to Prandtl's picture. Point (2) is related to the often overlooked finding of Chorin & Bernard (1973) that for a certain choice of time step, point vortices and vortex blobs gave similar results. We present results using Euler's method with several different ratios of $\vartheta = \frac{\Delta t}{\Delta \Gamma}$ which show irregularities for small ϑ although a complete understanding of this issue is lacking.

The third phenomenon is precisely the singularity formation discovered by Moore (1979) and Meiron, Baker & Orszag (1982). In section 2 Rosenhead's method is used to confirm some of their results. For the choice $\Delta t = \frac{1}{N}$ using Euler's method, we demonstrate convergence of the point vortex approximation at the critical time. A physical interpretation of the singularity formation, in terms of the strain rate along the sheet, is given in section 3 along with a description of the velocity field. Section 4 presents results showing an unexpected double roll up for certain initial conditions. We study the effect of changing the initial amplitude and present point vortex results in agreement with Moore's asymptotic relation for the critical time. Various issues are discussed in section 5. We assert, in contrast to the previous investigators' conclusion, that the formation of the singularity does

not necessarily invalidate the vortex sheet model. However, it does raise theoretical questions about the validity, possibly in a weak sense, of a nonanalytic vortex sheet. It also explains the failure of those numerical methods for the present problem which were based on the sheet's presumed analyticity.

Our work explains some of the previous negative numerical results for Kelvin-Helmholtz instability with analytic initial data and restores credibility to the point vortex approximation. This should not be taken as an endorsement of point vortices either for other vortex sheets or for more general problems of vortex dynamics.

1. The Role of Roundoff Error

As explained in the Introduction, the point vortex positions $\{Z_j(t), j=1, \ldots, N\}$ may be viewed as approximately interpolating the exact vortex sheet $Z(\Gamma, t)$ at points $\{\Gamma_j\}$. The perturbation, $P(\Gamma, t) = Z(\Gamma, t) - \Gamma$, is periodic in Γ with period 1 and it is therefore natural to consider $P_N(\Gamma, t)$, the trigonometric polynomial of degree $N-1$ which interpolates $\{P_j(t) \equiv Z_j(t) - \Gamma_j\}$ at $\Gamma = \Gamma_j$ for $j=1, \ldots, N$. A discrete Fourier transform is required in general to obtain the coefficients, $\hat{P_N}(k, t)$, of $P_N(\Gamma, t)$:

$$\hat{P}_N(k, t) = \sum_{j=1}^{N} P_j(t) e^{2\pi i k \Gamma_j} \quad , \quad k = -\frac{N}{2}, \ldots, \frac{N}{2} - 1 .$$

However, in our problem, the fast Fourier transform (FFT) (IMSL 1982) can be used since the $\{\Gamma_j\}$ are equally spaced on [0,1]. We expect that $P_N(\Gamma, t)$, given explicitly by:

$$P_N(\Gamma, t) = \frac{1}{N} \sum_{k=-\frac{N}{2}}^{\frac{N}{2}-1} \hat{P}_N(k, t) e^{-2\pi i k \Gamma},$$

approximates the exact perturbation for all values $0 \leq \Gamma \leq 1$. Similar formulae are available when N is an odd integer. The vortices will be connected by plotting the interpolating curve $P_N(\Gamma, t) + \Gamma$ as a function of Γ.

A solution to the point vortex equations (0.4) with $N=100$ was obtained by Euler's method using $\Delta t = 0{\cdot}01$. The initial condition was a discretized linear theory growing mode of amplitude $\alpha = 0{\cdot}01$ and wavelength 1 (see (0.3a))

$$Z(\Gamma_j, 0) = \Gamma_j + \alpha(1 - i)\sin 2\pi\Gamma_j \quad , \quad \Gamma_j = (j-1)/N . \qquad (1.1)$$

This computation was performed in double precision on a VAX 11/780 computer giving 14 digits of precision.

The right side of figure 1.1 shows the vortex positions at successive times and the left side shows the corresponding interpolating curves. The vortices tend to form pairs and larger clusters which exhibit irregular small scale motion similar to that seen by many numerical investigations of Kelvin-Helmholtz instability after Rosenhead's. The resulting vortex sheet quickly tangles and the computation's reliability deteriorates.

Figure 1.2 displays linear-log plots of the computed Fourier coefficients' amplitudes $|\hat{P}_N(k,t)|$, as a function of wavenumber k, for $0 \le t \le 0{\cdot}5$ in steps of $0{\cdot}05$ and at $t = 1$. All of the initial conditions considered in this paper will satisfy $P(-\Gamma, 0) = -P(\Gamma, 0)$, a property that is preserved under evolution and discretization. This implies that $\hat{P}_N(-k,t) = -\hat{P}_N(k,t)$ and therefore only Fourier coefficient amplitudes for $0 \le k \le k_{\max}$, $k_{\max} = \frac{N}{2} - 1$ appear in our spectral plots. The perturbation in initial condition (1.1) has, for $0 \le k \le k_{\max}$, only one nonzero discrete Fourier coefficient, $\hat{P}_N(k=1, t=0) = a(1-i)$. Figure 1.2 shows the computed initial spectrum which contains the spike at $k=1$ and small amplitude numerical noise ($\approx 10^{-13}$) in all the higher modes. This is not surprising and is due to roundoff error in setting up the initial condition and in the FFT. A horizontal line drawn at amplitude $\ln 10^{-13} \approx -30$ bounds the noise level of the computation.

As time progresses, the spike spreads out in frequency space and the higher modes grow in amplitude. For $t \le 0{\cdot}1$, the logarithmic amplitudes decrease linearly with increasing wavenumber until they fall below and remain bounded by the noise level out to $k_{\max}$. This accords with the common notion of nonlinear excitation of frequencies.

By $t = 0{\cdot}15$ something unexpected has happened. The previous behaviour is repeated for $k < 25$ while a wiggly tail of amplitudes has

emerged just above the noise level for $25 < k < k_{max}$. The highest wavenumber modes grow fastest out of the noise, recalling the dispersion relation of linear Kelvin-Helmholtz instability. For $0{\cdot}2 \leq t \leq 0{\cdot}45$ the spectrum has a low wavenumber band with monotone decreasing amplitudes and a high wavenumber band with roughly increasing amplitudes. This behaviour in the spectrum's tail indicates a nonanalytic solution. It appears that before the highest modes are amplified by nonlinearity, they are subject to linear Kelvin-Helmholtz instability. The roundoff error supplies a perturbation to all modes which conspires with linear instability to amplify the high wavenumber modes above the noise level. For $0{\cdot}2 \leq t \leq 0{\cdot}45$ these modes grow in time at a uniform rate, presumably due to finite amplitude effects, leading to the irregular vortex motion of figure 1.1 .

To understand what would happen if k_{max} were smaller, i.e. using fewer point vortices, draw a vertical line in figure 1.2 and ignore everything to its right. If the line is drawn to the left of $k = 25$, the premature growth of high wavenumber modes does not occur. This is because nonlinearity reaches this lower k_{max} before linear instability can amplify $\hat{P}_N(k_{max}, t)$ above the noise level. We have observed this in computations using $k_{max} = 20$ which produce a smooth roll up similar to Rosenhead's. If k_{max} is increased, linear instability acts on higher wavenumber modes causing them to grow more rapidly. Thus the increasingly "chaotic" small scale behavior previously observed as more vortices were used is a numerical phenomenon which originates in finite precision arithmetic.

This assertion is consistent with Moore's (1981) finding for the circular vortex sheet. Instead of seeking ways to dampen the short wave instability, as he did, we prefer to focus attention on reducing the amplitude of the numerical noise. We believe that for arbitary values of N and any consistent time integration scheme, approximate solutions to the point vortex equa-

tions (0.4) with initial condition (1.1), will not exhibit this "chaotic" motion if the arithmetic is sufficiently precise.

One way to test this conjecture is to compute with more digits of accuracy. Before presenting these results, an alternative procedure for controlling the spurious perturbing of the higher modes will be described.

From the noise level of the computed initial condition seen in figure 1.2, it is clear that the computation cannot distinguish between a mode of zero amplitude and one of amplitude roughly 10^{-13}. Therefore at the end of every time step we reset to zero any Fourier coefficient whose amplitude is less than 10^{-13}. The vortex positions are then correspondingly adjusted by an inverse FFT and the calculation proceeds to the next time step. In order for a mode to grow, its amplitude must therefore jump above the noise level in a single time step.

Figure 1.3 shows the result of implementing this chopping procedure in a computation which is otherwise identical to that which produced figures 1.1 and 1.2 . For $0{\cdot}5 \leq t \leq 1{\cdot}5$, the vortex sheet rolls up smoothly into a spiral. Past $t = 1{\cdot}5$, two types of irregularity appear in figure 1.3 :

(1) Small scale vortex pairing occurs on the almost flat portion of the sheet between adjacent vortex cores, the "braid" region. This version of linear Kelvin-Helmholtz instability is inhibited by the strain field induced by the neighboring cores and thus occurs on a slow time scale. This irregularity also originates in perturbations introduced by roundoff error as will be demonstrated shortly. The chopping procedure cannot be applied because by this time ($t \geq 1.5$), the spectral amplitudes have grown above the noise level. It is not clear how to filter numerical noise from these nonzero Fourier coefficients without making ad-hoc assumptions. The strain field and its suggestion of finite amplitude stability will be discussed in greater detail in section 3.

(2) The spacing between adjacent turns in the spiral becomes smaller than the spacing between consecutive vortices. Thus vortices on different spiral turns which happen to lie close to one another capture each other and rotate in pairs. The resulting distortion and tangling of the inner turns of the spiral are due to the truncation errors of the Γ and t discretizations and not to the roundoff amplification of point (1) above. The smooth portions of the outer turns are presumably still an accurate representation of the exact solution. The tangling slowly spreads to include more spiral turns.

Figures 1.4a,b display linear-log and log-log plots of the spectral amplitudes corresponding to figure 1.3 . The chopping procedure has eliminated the amplification of numerical noise seen in figure 1.1 while allowing the higher modes to grow in an orderly manner. For $t \leq 0{\cdot}5$, the computed spectrum decays monotonically. In section 2 this decay is analyzed and conclusions are drawn concerning the analytic structure of the vortex sheet. We point out that the chopping procedure operates only during the time interval $[0, 0{\cdot}38]$, the time taken for nonlinearity to amplify $\hat{P}_N(k_{\max}, t)$ above the noise level, beyond which the program reverts to the standard point vortex method.

In order to further test our ideas about the role of roundoff error, program was run, with the chopping procedure turned off, in double precision on a CDC 7600 giving 29 digits of precision. Figure 1.5 shows the resulting vortex sheet. The corresponding spectrum is virtually indistinguishable from figures 1.4a,b and so is not shown. Now the braid region remains smooth even for long times. In this run, linear instability acts upon modal perturbations of smaller amplitude than in the 14 digit calculation. Spurious growth of higher modes occurs here too, but starting from a lower noise level, it never affects the solution plotted in figure 1.5 . Calculation with

high enough values of N does produce irregular vortex motion even for 29 digits of precision. The core regions of figure 1.5 are identical to those of figure 1.3, supporting the claim that the tangling there is not due to roundoff amplification.

A plot of vortex trajectories is given in figure 1.6 . The vortex sheet is plotted at $t=0{\cdot}46$, just when roll up begins. According to linear theory for a single mode solution, material points move on straight lines inclined 45° to the horizontal axis (see (0.3)), as observed in this plot for short time, $t<0{\cdot}46$. For longer times, vortices near the sheet's center ($\Gamma=0{\cdot}5$) move in spiral orbits while vortex trajectories near $\Gamma=0,1$ are still fairly straight. Evidently, the linear theory breaks down nonuniformly in $\Gamma-t$ space.

The existence of certain invariants offers a check on aspects of the computation's accuracy. For a periodic array of point vortices (0.4a) the mean vortex position,

$$Z_m(t) = \frac{1}{N}\sum_{k=1}^{N} Z_k(t)\,,$$

and the Hamiltonian (0.5) are constant and serve as a check on the ODE solver. The computed mean position was preserved to high accuracy. A plot of the computed Hamiltonian is given in figure 1.7 . The mean relative variation in $H_{100}(t)$ per time step was $\left|\dfrac{H_{100}(4)-H_{100}(0)}{H_{100}(0)\cdot 4/\Delta t}\right| \approx 0{\cdot}005$, a reasonable accuracy for first order time integration with $\Delta t=0{\cdot}01$.

An effort was made to assess the importance of a more familiar roundoff effect, namely loss of significant digits due to cancellation. In the interaction velocity calculation of equation (0.4a), expressed in real and imaginary parts, the denominator

$$\cosh(2\pi(Y_j-Y_k)) - \cos(2\pi(X_j-X_k))\,,$$

was replaced by the equivalent

$$2(\sinh^2(\pi(Y_j-Y_k)) + \sin^2(\pi(X_j-X_k)))\,, \quad \text{where } Z_j = X_j + iY_j\,,$$

as suggested by Van de Vooren (1965, pub. 1980). We also tried various implementations of the Biot-Savart summation in (0.4a) including Kahan's algorithm (Dahlquist 1975) for controlling loss of significance, and symmetric summation. In the latter, interaction velocities with indices $k = j \pm l$ are summed in pairs and the resulting terms are summed in increasing magnitude. None of these devices had any significant effect on the computed results.

Since the erratic small scale motion previously observed in computations with a large number of point vortices for this problem can be controlled, it becomes reasonable to inquire into the convergence properties of the approximation. Figures 1.8a,b show the evolution for $N = 20$ using Euler's method with Δt between 0·1 and 0·005 and then using 4^{th} order Runge-Kutta with $\Delta t = 0{\cdot}05$. As the truncation error due to the time integration becomes smaller, the approximate votex sheets converge to a curve with a tangled core. We observed this for several different values of N and conclude that it is a property of exact solutions of the point vortex equations (0.4).

Such tangling is not expected for solutions of the continuous equations (0.2). In fact, the invariance of the continuous system's Hamiltonian, (0.6) implies that a continuous vortex sheet cannot cross itself unless the vortex sheet strength is also zero at the point of intersection. The invariance of the discrete system's Hamiltonian, (0.5) only precludes the arbitrarily close approach of point vortices and imposes no obvious constraint on the approximate vortex sheet constructed from those vortices.

These remarks suggest that the *exact* evolution of a finite number of point vortices is not a particularly accurate approximation to the vortex sheet evolution under consideration. If this is true then the common

practice of previous investigators in solving the point vortex equations (0.4) very accurately has been self-defeating. It may be that the *approximate* evolution of a finite number of point vortices gives a better approximation to the continuous vortex sheet. Some of our calculations using Euler's method and large Δt give plausible approximations to the physically observed smooth roll up. The smoothing effect of large time steps was noted by Chorin & Bernard (1973) in the context of a different vortex sheet.

2. The Formation of a Singularity

The point vortex method is used in this section to study the formation of a singularity in the vortex sheet. Sulem, Sulem & Frisch (1983) (referred to later as SSF) showed that pseudospectral numerical methods can detect the analytic structure of periodic solutions of nonlinear evolution equations up to the time a singularity occurs. This approach will be explained and then applied to the point vortex results.

Consider an evolution equation for which real analytic initial data is given. A basic mathematical issue is whether or not "breakdown", i.e. loss of analyticity, occurs in a finite time. A simple example of breakdown is the development of shocks for the inviscid Burgers equation with periodic analytic initial data. The analytic continuation into the complex plane of the real analytic solution will generally have complex singularities. As the solution evolves, each singularity traces a curve in the complex plane. One view of breakdown is that such a curve intersects the real axis in a finite time. To detect this, SSF exploited the relation between the analytic properties of a function and the high frequency asymptotic behaviour of its Fourier transform (Carrier, Krook & Pearson 1966).

Suppose that for Γ in a complex neighborhood of $\Gamma_0(t) + i\delta(t)$, the function $P(\Gamma, t)$ has the behaviour :

$$P(\Gamma, t) \sim (\Gamma - (\Gamma_0(t) + i\delta(t)))^{\mu(t)}, \tag{2.1}$$

where Γ_0 is real, $\delta > 0$ and $\mu > -1$. If this branch point is the closest singularity to the real axis in the upper half plane, then the Fourier coefficients of P decay asymptotically for $k \to \infty$,

$$\hat{P}(k, t) \sim k^{-(\mu(t)+1)} e^{-k\delta(t)} e^{ik\Gamma_0(t)}, \quad k \to +\infty. \tag{2.2}$$

The exponential decrement $\delta(t)$ is the width of the analyticity strip in the

upper half plane and $\mu(t)$ is the order of the branch point.

Pseudospectral solution of the evolution equation yields approximate values of $\hat{P}(k,t)$ at each time step. Sulem, Sulem & Frisch proposed estimating $\mu(t)$ and $\delta(t)$ by least squares fitting of the model (2.2) to the approximate spectrum computed in this way. A narrow band of wavenumbers adjacent to k_{max} was excluded from the fit since these were thought to be inaccurate due to series truncation effects. Fourier coefficients whose amplitudes are in the noise level are not described by (2.2) and were also excluded. Numerical evidence for global time analyticity is obtained if the fitted $\delta(t)$ remains positive. Alternatively, breakdown may be deduced if $\delta(t)$ equals zero within the computation's resolution at a finite time t_c. At the critical time t_c, the spectrum decays algebraically and the fitted $\mu_c = \mu(t_c)$ tells how many derivatives the solution retains. For example, if $1 < \mu_c < 2$ then $P(\Gamma, t_c)$ has a continuous first derivative but its second derivative is undefined at $\Gamma_0(t_c)$.

Sulem, Sulem & Frisch pointed out that these estimates of the critical values, t_c and μ_c, depend on the range of computed Fourier coefficients included in the least squares fit. For the shock solution of Burgers equation which they studied, exponential decay $e^{-k\delta(t)}$ persists up to t_c in the high wavenumbers while power law decay $k^{-(\mu(t_c)+1)}$ at t_c dominates the low wavenumbers. These authors therefore use a high wavenumber band to estimate t_c and a low wavenumber band for μ_c and obtain agreement with the known critical values. The uncertainty in the method's estimates of critical values has not been rigorously analyzed and caution seems advised when interpreting the results for solutions of equations whose analytic structure is sought. This issue is discussed by Brachet, et. al. (1983) who applied the method to the Taylor-Green flow.

For the reasons outlined in the Introduction, it was commonly believed that Rosenhead's method was incapable of capturing the analytic properties of Kelvin-Helmholtz instability. Moore (1979) and Meiron, Baker & Orszag (1982) (referred to later as MBO) therefore employed asymptotic, analytic and alternative numerical techniques to compute Fourier coefficients for the vortex sheet from which conclusions were made using the model (2.2). For initial condition, Moore used a transverse sinusoidal perturbation and MBO used a flat vortex sheet with sinusoidally perturbed strength.

In spite of differences in initial conditions and methodology, both investigations revealed essentially the same phenomena :

(1) A singularity forms in a finite time which depends upon the initial amplitude. An explicit asymptotic relation for this dependence was given, valid for small amplitudes.

(2) The algebraic decay rate at the critical time is $\mu_c = 1{\cdot}5$ (Moore), $\mu_c = 1{\cdot}7 \pm 0{\cdot}2$ (MBO). This implies that the sheet's curvature becomes undefined at some point. The sheet however retains a Hölder continuous tangent vector at all points.

(3) When the singularity forms, the vortex sheet strength has a cusp although the sheet shows no sign of roll up.

These phenomena (except for the last part of (3)) will now be confirmed by using the point vortex method, with roundoff perturbation controlled, to calculate approximate values of $\hat{P}(k,t)$, as explained in section 1, and then estimating the critical values as described above. Concerning (3), it will be shown that the singularity time marks the beginning of a small scale roll up that could not have been noticed by the methods of Moore and MBO.

Recall that the initial condition used in our work is a discretized growing mode of linear theory (1.1). The almost straight lines in figure (1.4a) for

short times, $t < 0{\cdot}45$, and high wavenumbers, $k > 15$, indicate that the computed spectrum decays exponentially as a function of k. As t increases from 0 to 0·45, algebraic decay appears in the lower wavenumbers and gradually spreads to cover a wider band of frequencies (note the almost straight lines in figure 1.4b). This behaviour is consistent with the hypothesis that a complex singularity of $P(\Gamma, t)$ is approaching the real axis. We have implemented the least squares fit by transforming (2.2) to :

$$\ln|\hat{P}(k,t)| \sim -(\mu(t)+1)\ln k - \delta(t)k + C, \qquad (2.3)$$

which is linear in $\ln k$ and k. In the following, a superscript N (e.g. t_c^N), will denote a calculated value based on N point vortices per wavelength using Euler's method with a time step of $\Delta t = \frac{1}{N}$. A symbol with superscript ∞ (e.g. μ_c^∞) will denote a value extrapolated to $N \to \infty$.

Plotted in figures 2.1a,b are the computed $\delta^{100}(t)$ and $\mu^{100}(t)$ using model (2.3) fitted to several high wavenumber ranges. The width of the double line in figure (2.1a) is the smallest resolvable wavelength for this computation, $\frac{2\pi}{k_{\max}}$. The computed $\delta^{100}(t)$ approaches zero linearly and the critical time, taken as the first time step for which $\delta^{100}(t) < \frac{2\pi}{k_{\max}}$, is estimated as $t_c^{100} = 0{\cdot}46$. The accuracy of this value could be improved slightly by using linear approximation to determine when $\delta^{100}(t) = \frac{2\pi}{k_{\max}}$. This situation contrasts with that for the inviscid Taylor-Green vortex (Brachet, et.al. 1983) in which the exponential decrement approaches zero exponentially making determination of t_c a more delicate matter. Changing the band of fitted wavenumbers had only a small effect on $\delta^{100}(t)$ as long as a band of high wavenumbers was included.

Relying on the findings of SSF, to study the low wavenumber power law we will exclude the exponentially decaying high wavenumbers from the fit.

Plotted in figures 2.2a,b are $\delta^{100}(t)$ and $\mu^{100}(t)$ using model (2.3) fitted to several low wavenumber ranges including $1 \le k \le 15$, the range used by MBO in obtaining result (2) above. A value of $\mu_c^{100} = 1{\cdot}11$ based on this range is observed. The estimated value of μ_c depends on the range of low wavenumbers used in the fit and we cannot ascribe special significance to any of the particular values in figure 2.2b . We believe however that $1 < \mu_c < 2$ and find support for this in the plots of vortex sheet strength to be presented below.

Since the computed critical time and algebraic decay rate depend on N, the calculation was repeated for eight values of N between 50 and 400. Table 2.1 records these results and figures 2.3a,b plot the computed t_c^N and μ_c^N as functions of $\frac{1}{N}$. The curve drawn in these figures is a least squares fit of the eight data points to a quadratic model. The good fit obtained is evidence for the existence of constants, t_c^∞ and μ_c^∞, to which t_c^N and μ_c^N converge asymptotically,

$$t_c^\infty \sim t_c^N + \frac{c_1}{N} + \frac{c_2}{N^2} + \cdots \quad , \qquad \text{for } N \to \infty \text{ when } \Delta t = \frac{1}{N},$$

and similarly for μ_c^N . The constants $c_1, c_2, \ldots$ depend on the initial condition but are independent of N. Extrapolated values obtained from these curves are $t_c^\infty = 0{\cdot}38$ and $\mu_c^\infty = 1{\cdot}9$.

This critical time is less than that, 0·68 in our units, predicted by Moore's asymptotic relation. This is due to the difference in initial conditions whose effect upon the evolution will be discussed in section 4. The algebraic decay rate obtained here supports the conclusion in (2) concerning the regularity of the sheet at the critical time. The theoretical and numerical significance of this aspect of the singularity will be discussed in section 5.

Figure 2.4 shows the numerical solution using $N = 250, \Delta = 0{\cdot}004$ at successive times in a neighborhood of the critical time, $t_c^{250} = 0{\cdot}416$. A closeup view of the core is plotted together with the vortex sheet strength as a function of Γ, computed by pseudospectral differentiation. The critical time coincides with the formation of a cusp in the vortex sheet strength as observed by the previous investigators (point (3) above). Contary to their findings, we observe that roll up on a very small scale also begins at the critical time. Because the vortex sheet remains continuously differentiable at t_c, the ensuing roll up appears "smooth".

Figure 2.5 displays the vortex sheet strength as the cusp developes. In the core ($\Gamma \approx 0{\cdot}5$) the strength increases monotonically as $t \to t_c^{250}$ from below. Most of the growth in the cusp's amplitude takes place very close to the critical time.

3. Some Physical Properties of Roll Up

This section uses the computational results of section 1 to display various physical properties of the vortex sheet evolution including the strain rate along the sheet, growth of the sheet's arclength, streamlines of the induced velocity field and the maximum sheet displacement. Strain rate and arclength have been identified as important parameters in combustion problems (Ghoniem, Chorin & Oppenheim (1982)).

Corcos & Sherman (1983) have studied the tangential strain felt by a passive material curve in a viscous shear layer. The scalar strain rate γ was defined to be the proportional rate of extension along the curve:

$$\gamma = \lim_{dl \to 0} \frac{1}{dl} \frac{\partial (dl)}{\partial t} = \frac{\partial u_s}{\partial s}, \tag{3.1}$$

where dl is a Lagrangian curve element, u_s is the curve's tangential velocity and $\partial / \partial s$ means differentiation with respect to arclength. Positive values of γ imply local stretching of the material curve and negative values imply local compression. These authors presented a contour plot of γ as a function of time and of a Lagrangian curve parameter. The success of this approach in yielding a deeper understanding of shear layer dynamics has motivated the present study of the strain rate along the vortex sheet.

The viscous shear layer studied by Corcos and Sherman had, at $t = 0$, a continuous vorticity distribution. The vortex sheet model can be heuristically viewed as the limit in both vanishing viscosity and initial layer thickness. Comparison of the strain rates in the two studies offers some insight into the nature of this dual limit.

For the vortex sheet, γ can be expressed as :

$$\gamma(\Gamma, t) = \mathrm{Re}(\sigma (\sigma Z_\Gamma \overline{Z}_t)_\Gamma), \quad \mathrm{Re} \equiv \text{real part}. \tag{3.2}$$

This follows from (3.1) since the real and imaginary parts of σZ_Γ form a unit

vector tangent to the vortex sheet and $\partial/\partial s = \sigma\,\partial/\partial\Gamma$. Pseudospectral approximation of γ by this expression should be very accurate up to the critical time. Alternatively, one may approximate expression (3.1) by:

$$\gamma((j+\tfrac{1}{2})\Delta\Gamma, n\Delta t) \approx \frac{1}{|Z_{j+1}^n - Z_j^n|} \frac{|Z_{j+1}^n - Z_j^n| - |Z_{j+1}^{n-1} - Z_j^{n-1}|}{\Delta t}, \qquad (3.3)$$

where Z_j^n is the position of the j^{th} point vortex at time $n\Delta t$. Figure 3.1a shows a contour plot of $\gamma(\Gamma, t)$ over the half period $0 \le \Gamma \le 0{\cdot}5$ up to $t=1$ and figure 3.1b is a closeup plot for $0{\cdot}4 \le \Gamma \le 0{\cdot}5$ and $0{\cdot}4 \le t \le 0{\cdot}5$. The plotting routine has left white space in regions where the contour lines are very close. Figures 3.2a-d show $\gamma(\Gamma, t)$ for $\Gamma = 0, 0{\cdot}25, 0{\cdot}45, 0{\cdot}5$ as functions of time up to $t=4$. These values of γ were computed by the finite difference expression (3.3). The corresponding vortex sheet was shown in figures 1.3 and 1.5.

The most prominent feature of these plots is the discontinuous strain rate at the interface's center, $\Gamma = 0{\cdot}5$. A global minimum in Γ, t space of $\gamma \approx -20$ occurs at the critical time ($t_c^{100} = 0{\cdot}46$) and a global maximum of $\gamma \approx +40$ occurs one time step later. Computations with increasing values of N showed an increasing jump in γ at t_c^N from negative to positive values. In their study, Corcos and Sherman found a continuous strain rate with global extrema roughly ± 10 (in our units) in the core around the time at which the material curve achieved a vertical slope. As expected, viscosity and finite layer thickness at $t = 0$ produced a less fierce roll up than does the inviscid vortex sheet model.

Examination of figures 1.3 (for $t = 0{\cdot}4$), 3.1 and 3.2 reveals that up to the critical time, negative strain near $\Gamma = 0{\cdot}5$ pulls point vortices closer together and into the core region. This compression at the center causes the outer portions of the sheet to stretch. For example at $t=0$, 50% of the sheet ($0{\cdot}25 < \Gamma < 0{\cdot}75$) is stretching while this fraction increases to 80%

$(0<\Gamma<0{\cdot}4, 0{\cdot}6<\Gamma<1)$ by $t=0{\cdot}4$. For the viscous, finite initial thickness layer the opposite was observed, i.e. before roll up, more and more of the interface was compressed though to a lesser degree than seen here. Professor Corcos conjectures this is due primarily to finite initial thickness rather than nonzero viscosity.

In our problem, the concentration of vorticity and negative strain rate at the sheet's center are resolved at the critical time when the vortex sheet "cracks" (curvature discontinuity of section 2) leading to the large positive strain rate just past t_c^N. Beyond the critical time the strain rate oscillates both in time and along the interface in qualitative agreement with the results of Corcos & Sherman. Figures 3.1a,b indicate a predominance of positive strain rates, with the braid region ($\Gamma\approx 0, 1$) being continuously stretched for long times. Figure 3.3 shows the resulting increase of the sheet's arclength. To obtain this plot, the arclength element ds was approximated by the chordlength $|Z_{j+1}-Z_j|$ of consecutive point vortices. Up to t_c^N the arclength hardly grows, but it increases linearly with time afterwards. This was observed using other values of N with larger rate of increase of arclength for larger N. The numerical results do not rule out the possibility that the continuous vortex sheet developes infinite arclength past t_c.

Another effect of the predominantly positive strain rates beyond t_c^N is to smooth out small amplitude short wavelength perturbations in sheet position. This was already observed numerically in section 1 in connection with the slow irregular motion of point vortices in the braid region for the 14 digit calculation (figure 1.3). It appears that the singularity has a stabilizing effect on the vortex sheet evolution. The relation between vortex sheet stretching and stability has been studied by Moore (1976). The stabilizing effect of a singularity is known for shock waves (Lax 1973) and has also been observed recently in cusp formation for a model of flame propagation

(Sethian 1982).

Streamlines are an important visual aid to understanding two dimensional incompressible fluid flow. For a periodic vortex sheet $Z(\Gamma,t)$, the stream function at an aribtrary point z not on the sheet is given by:

$$\psi(z,t) = \frac{-1}{2\pi}\int_0^1 \ln\,|\sin\pi(z - Z(\Gamma,t))|\;d\Gamma\,. \tag{3.4}$$

This integral is a simple layer of strength $\sigma = \frac{d\Gamma}{ds}$, the vortex sheet strength (Kellogg 1953). Away from the vortex sheet the integral is proper and ψ is harmonic. Both the stream function ψ and the tangential derivative $\frac{\partial\psi}{\partial s}$ are continuous across the sheet while the normal derivative $\frac{\partial\psi}{\partial n}$ has a jump discontinuity equal to σ. Trapezoidal quadrature of the integral in (3.4) yields the stream function $\psi_N(z,t)$ of a set of periodic point vortices:

$$\psi(z,t) = \frac{-1}{2\pi N}\sum_{k=1}^{N} \ln\,|\sin\pi(z - Z_k(t))|\,. \tag{3.5}$$

If $z = Z_j(t)$ for some index j then the summation above should omit $k=j$.

Contour plots of ψ at successive times were obtained using approximation (3.5) and are displayed in figures 3.4a-h. The contour lines have deliberately not been smoothed in order to display the jump in $\frac{\partial\psi}{\partial n}$ across the vortex sheet. To avoid seeing the circular streamlines close to the point vortices, ψ_N was evaluated on a coarse mesh (35 by 35). The contour plotting routine has difficulty resolving the saddle points $\Gamma = 0, 1$ of the stream function and the plots should not be taken literally near these points. Such errors in these contour plots could be diminished by using the trigonometric interpolating curve to obtain a more accurate evaluation of the integral in (3.4) than that given by (3.5).

Streamlines intersecting at $\Gamma = 0, 1$ separate an unbounded region of open streamlines away from the interface from a bounded region of closed streamlines surrounding the interface. This latter region of recirculating fluid (dubbed "cat's eyes" by Kelvin) allows the two fluid streams to mix. For roughly $t < 3$, fluid continuously has crossed the cat's eye boundary, entering the bounded region and causing its area to increase.

Figure 3.5 shows the computed maximum sheet amplitude, $Y_{max}(t)$ plotted against time. Exponential increase occurs up to $t \approx 0{\cdot}46 = t_c^{100}$ followed by an interval of approximately linear increase $t_c^{100} < t < 3$. The bumps in amplitude appearing for later times are due to the tangling of the sheet's turns. For $t > 3.5$ the rolled up sheet is shrinking in amplitude but increasing its streamwise extent extent.

At late times ($t \approx 4$) the recirculation region stops growing and the closed streamlines assume an elliptical concentric pattern which flattens in the streamwise direction. For $t < 4$ the vortex sheet remains inside the cat's eye. At $t = 4$ it appears that some portion of the vortex sheet crosses the cat's eye boundary into the streaming fluid. In a real shear layer, further growth can take place through pairing of adjacent vortex cores as observed experimentally by Winant & Browand (1974). This long wave instability contrasts with the short wave stability (after roll up) indicated above. Patnaik, Corcos & Sherman (1976) numerically studied vortex pairing in a viscous shear layer by including a subharmonic linear theory eigenfunction in the initial condition. This could also be done for the present vortex sheet model.

4. The Effect of Varying the Initial Condition

In this section we will first make some general remarks concerning our choice of initial condition (1.1) and then study numerically how different initial conditions effect some properties of the evolution. All computations presented in this section were performed with $N = 250$, 29 digits of accuracy, the chopping procedure turned on at the level 10^{-25} and Euler's method with $\Delta t = 0{\cdot}004$.

The vortex sheet model under study has two components, namely the evolution equation and the initial condition. It is reasonable to require some degree of consistency between these components. Mathematically this means that the initial condition should belong to some class of functions for which the initial value problem is well posed for at least a finite time. Sulem, Sulem, Bardos, & Frisch (1981) have shown that a class of analytic functions, bounded in a certain norm, meets this requirement. One also seeks to determine those initial conditions which approximate a physically interesting situation and which do not violate the modelling assumptions implicit in the evolution equation. Since the vortex sheet is essentially a long wave approximation to a shear layer of finite thickness, we would not expect to obtain meaningful results from initial conditions which contain arbitrarily short wavelengths of large amplitudes. This gives heuristic credibility to the mathematical well posedness result mentioned above. The fact that by a finite time the evolution equation has amplified the short wavelengths in a particular way is not inconsistent with the need to restrict the size of these short wavelengths in the initial condition.

Experimental observation should also guide the choice of initial condition. Corcos & Sherman (1983), citing the experiments of Thorpe (1971), have emphasized that shear layers exhibit a sharp selection mechanism

which initially inhibits the growth of all but a single dominant wavelength. While this mechanism needs further study, it motivates our use, in the vortex sheet model, of a growing eigenfunction of linear theory with small amplitude to wavelength ratio as the initial condition. This choice yields a model which is mathematically consistent and that we hope has physical content.

Consider the following initial conditions:

$$Z(\Gamma,0) = \Gamma + \alpha(1-i)\sin 2\pi\Gamma\,, \tag{4.1}$$

$$Z(\Gamma,0) = \Gamma + \alpha i \sin 2\pi\Gamma\,. \tag{4.2}$$

The right side of (4.1) is a linear theory growing mode whose complex conjugate is a decaying mode (see 0.3a,b). The transverse sinusoidal perturbation (4.2) considered by Moore (1979) is a linear combination of growing and decaying modes of equal amplitude.

We pose the following questions :

(1) The numerical results presented thus far have used initial condition (4.1) with $\alpha = 0{\cdot}01$. What effect does changing the initial amplitude have on the evolution?

(2) How do solutions using (4.2) compare with those using (4.1)?

(3) Using (4.2), Moore derived the following asymptotic relation between the critical time t_c and the initial amplitude α (expressed in our units):

$$1 + \pi\tau_c + \ln 2\pi\tau_c = \ln\frac{2}{\pi\alpha}, \tag{4.4}$$

$$t_c = \tau_c + \frac{1}{2\pi^2\tau_c} + \frac{29}{48\pi^3\tau_c^2} + \cdots \quad , \quad \alpha \to 0\,.$$

How well do point vortex solutions using (4.2) agree with this result?

To answer the first question, computations using (4.1) were performed for values of a between 0·0025 and 0·08. In all cases it was observed that smaller a led to smaller $Y_{max}(t_c)$ and larger t_c. For values of a less than approximately 0·04, the evolution was generally similar to what has already been described for $a = 0{\cdot}01$. Initial amplitudes larger than 0·04 produced some significant differences. These are evident in figure 4.1 which shows the evolution using $a = 0{\cdot}08$.

First, point vortices crowd together along a portion of the core region forming approximately a straight line segment. At the critical time, two cusps have formed in the vortex sheet strength at positions corresponding to the straight segment's ends (figure 4.2). Then both ends roll up on a small scale and eventually merge. A plot of Fourier coefficient amplitudes (figure 4.3) reveals a modulation of the previous behaviour, $|\hat{P}(k)| \sim k^{-(\mu+1)}e^{-\delta k}$ up to t_c, which had been observed in section 1 for $a = 0{\cdot}01$. This modulation does not occur when a single branch point in the upper half plane approaches the real axis and must therefore be due to a more complicated distribution of complex singularities.

The evolution using (4.2) and $a = 0{\cdot}08$ is shown in figure 4.4 with the corresponding spectrum in figure 4.5 . Straightening and double roll up, similar to that of initial condition (4.1) for large a, was observed here for smaller initial amplitudes (e.g. even for $a = 0{\cdot}01$). Such behaviour was previously observed (see our figure 0.3a from Birkhoff & Fisher (1959)) and interpreted as irregularity. Now we can explain the double roll up as the outcome of sheet straightening which itself can be caused by large initial amplitudes or inclusion of a decaying linear mode in the initial condition. In computations using initial condition (4.2), a singularity developed later than for initial condition (4.1) with equal amplitude. It is plausible that this delayed critical time is due to an interaction between the growing and decaying

modes initially present in (4.2) .

For both initial conditions (4.1) and (4.2), as α becomes smaller, the two cusps approach $\Gamma = 0{\cdot}5$ until they cannot be distinguished from a single cusp. For (4.2) these cusps remain distinct for smaller values of α than for solutions using (4.1) . Whether two distinct cusps persist in the exact solution as $\alpha \to 0$ or bifurcate from a single cusp at some finite initial amplitude could not be determined by the present computations. Chorin (1983), in a numerical study of instability of fronts in porous media, has also observed qualitative changes when the initial perturbation amplitude is raised above a certain value. I cannot explain why the spectrum of figure 4.5 is so much less smooth than that of figure 4.3 . The modulated behaviour of Fourier coefficients for certain initial conditions makes critical time prediction by the method of Sulem, Sulem & Frisch (1983) less straightforward. This is because the simple model of spectral decay (equation (2.2)) is not strictly applicable. Alternatively, the critical time may be estimated by the occurence of several other related events: minimum separation of two point vortices, global minimum in strain rate along the sheet, cusp appearing in sheet strength.

Table 4.1 contains critical times which were collected in this way for various values of α and N, using initial conditions (4.1) and (4.2). Critical times $t_c^{\infty}(\alpha)$, extrapolated to $N \to \infty$ as in section 2, are plotted in figure 4.6 together with the first three approximations to $t_c(\alpha)$ given by Moore's asymptotic relation (4.4). For values of $\alpha = 0{\cdot}04, 0{\cdot}08$ the first term of (4.4) gives the closest agreement with our computed critical time. As α decreases to $0{\cdot}0025$, the first two terms and finally the first three terms give the closest agreement. These results are consistent with the asymptotic validity, as $\alpha \to 0$, of Moore's relation.

Figure 4.6 also shows that the critical time for the growing mode perturbation (4.1) is smaller than that for the less physically motivated (4.2). The critical time thus depends on both the initial perturbation's amplitude and its particular decomposition into linear theory eigenfunctions. Although both Moore's result and our point vortex computations lack rigorous justification, their agreement gives confidence in the reliability of these critical times.

5. Discussion and Conclusions

Rosenhead's classical numerical method for vortex sheet evolution from analytic initial data has been examined using the discrete Fourier analysis techniques of Sulem, Sulem & Frisch (1983), leading to a deeper but still incomplete understanding of Kelvin-Helmholtz instability and the point vortex approximation.

Previous investigations using a large number of point vortices have failed because short wavelength perturbations introduced by machine roundoff error grow exponentially fast during the linear instability stage of the evolution. This mechanism should be contrasted with loss of significant digits, a more familiar finite precision effect. This occurs for example when numbers of disparate magnitude are added or a number is divided by another of much smaller magnitude. Perturbations grow in the present case not by arithmetic accumulation of rounding errors but because of the model's dynamics.

If the exact initial perturbation is analytic then its high frequency amplitudes decrease exponentially fast with increasing wavenumber. The number of point vortices used is also the highest wavenumber resolved by the computation. With a large number of point vortices, this means that the computed discrete initial spectrum's high frequencies are dominated by computational noise and their amplitudes do not decay. The numerical evidence suggests that the high frequency modes grow in time either by amplification of roundoff error perturbations or by nonlinearity. The computational challenge is to suppress the former while not disturbing the latter.

We call attention to the numerically observed asymptotic nature of the relation between machine precision, number of computational elements and

the error in the computed solution. With more than a certain number of vortices, which depends on the machine precision, larger computational errors are incurred. This is because with more point vortices, shorter wavelengths are represented and once spuriously perturbed, amplify quicker, leading to faster collapse of the computation. For any number of point vortices, a sufficiently precise calculation will reduce this source of computational error. This is because with greater machine precision, the spurious short wave perturbations enter the computation at a lower amplitude. Past an amount which depends on the number of computational elements, extra precison has no significant effect on the computation. The precision necessary to decrease the computational noise to a harmless level increases sharply with the number of vortices.

The numerical phenomenon described above can be expected to occur for other physical models which exhibit linear short wave instability (e.g. Rayleigh-Taylor instability). The severity of the problem also depends on what is happening dynamically. For Kelvin-Helmholtz instability, an increase in the amplitude of the initial perturbation causes faster developement of a strain field whose predominant stretching stabilizes the roll up to small amplitude short wave perturbations. Conversely, with smaller initial amplitudes, the linear instability stage of the evolution is prolonged, allowing more time for the spurious perturbations to grow. We expect that the roundoff amplification problem would be diminished by the inclusion in the model of surface tension, finite initial layer thickness or viscosity which stabilize short wave perturbations according to linear theory.

Because high precision arithmetic is expensive, we have introduced a chopping procedure which allows more computational elements to be used for a given machine accuracy. The procedure is heuristically justified if the initial perturbation is analytic, making it easier to distinguish arithmetic

noise from the genuine high frequency component. Under such circumstances, chopping effectively forces the computed spectrum to have compact support for a finite time. During this time the computed solution approximates an analytic function in accordance with the theoretical result of Sulem, Sulem, Bardos & Frisch (1981). The chopping procedure turns off when nonlinearity has amplified all the modes above the noise level. Some of the vortex blobs currently used for other flows have Fourier transforms which decay at high frequencies (Chorin 1973 and Beale & Majda 1983). It may be that for the present problem, such computational elements will loosen the precision constraint with no drastic damage to the truncation error. Discrete Fourier analysis should be useful in testing this conjecture.

Our point vortex results confirm the formation of a singularity in finite time for analytic initial data as found by Moore (1979) and Meiron, Baker & Orszag (1982) using different techniques. For initial conditions (4.1) and (4.2), $Z(\Gamma, t)$ remains analytic at the critical time except at one or two values of Γ, corresponding to the centers of the roll up, where the sheet retains a Hölder continuous tangent vector. The Cauchy principal value integral in (0.3a) can still be defined for such a vortex sheet although the methods used by Moore and MBO rely on the sheet's analyticity and are formally valid only up to the critical time. I therefore disagree with the conclusion of Moore and Meiron, Baker & Orszag that this singularity's formation restricts the validity of the vortex sheet model at the critical time. The indications that past the critical time the sheet has an infinite number of turns, as conjectured by D. Pullin (private communication), and infinite arclength seem to pose difficulties for the proper definition of a Cauchy principal value integral. Infinite spiral vortex sheets with special structure have been studied asymptotically and numerically (see Pullin & Phillips (1981) for some recent work) and we hope to eventually relate these results to the present

work.

The formation of the singularity explains the difficulty encountered by the numerical methods of Van de Vooren (1965, pub. 1980) and Fink & Soh (1978) in studies of Kelvin-Helmholtz instability. These methods rely for their consistency on the existence of higher derivatives of the exact solution and even if the problem of roundoff amplification is circumvented, erratic sheet motion appears beyond the critical time. We have checked this by using Van de Vooren's correction (0.7) evaluated by pseudospectral differentiation in Γ. At the critical time, the correction term $(Z_{\Gamma\Gamma}/\, Z_\Gamma^2)_j$ becomes undefined at some point.

A standard objection to Rosenhead's method for vortex sheet evolution is that it neglects higher order terms associated with the integrand singularity in the Cauchy principal value integral (0.2a) (Fink & Soh 1978). Recall however the definition of such an integral as the limit as $\varepsilon \to 0$ of proper integrals for which a symmetric interval of length ε around the singularity has been removed. The omission of a velocity self interaction term in the summation (0.4a) is a subtle numerical implementation of this definition. Consistency of the trapezoidal quadrature, which was used in approximating (0.2a) by (0.4a), follows from the Hölder continuity of the vortex sheet strength. These considerations do not necessarily apply to vorticity distributed over two and three dimensional volumes for which the Biot-Savart integral is improper.

Up to the critical time, the vortices move approximately on straight lines implying that even Euler's method with a large time step is accurate. Past the critical time we have seen that reducing the time truncation error for fixed N leads to sheet tangling. We view this as evidence that the exact evolution of a finite number of point vortices does not describe with uniform accuracy the evolution of the particular vortex sheet under consideration.

We have observed more plausible behaviour using Euler's method with $\Delta t = \frac{\vartheta}{N}$ and $\vartheta \geq 1$. A complete understanding of the relation between the Γ and t discretizations is lacking and presents another interesting area for future research.

The formation of the singularity results from a concentration of vorticity and has dynamical significance. At the critical time, the tangential strain rate at some material point jumps from a large negative value to a large positive value as the sheet begins to roll up on a small scale. The ensuing roll up is stable to small amplitude short wavelength perturbations, in the sense that such perturbations do not grow drastically. This contrasts with the strong short wave linear instability before the critical time.

Birkhoff & Fisher (1959) noted the relevance of the Poincaré recurrence theorem (Thompson 1979) to the periodic point vortex equations (0.4). For the theorem to apply, the point vortices must remain in a bounded region of the configuration space. This is satisfied by using periodicity to identify point vortex arrays modulo integer shifts in the horizontal direction and assuming bounded motion in the vertical direction. The theorem says that almost every configuration will eventually return arbitrarily close to its initial configuration. Birkhoff & Fisher concluded that vortex sheets eventually have to unroll. Recall however that it is the configuration of point vortices as well as their ordering and the curve that connects them which determine the approximate vortex sheet. A particular vortex configuration may recur even though the vortex sheet has rolled up. The recurrence of the point vortex configuration does not mean that the sheet has returned to its initial shape.

We have demonstrated that information about vortex sheet instability can be obtained by using the point vortex approximation. A rigorous con-

vergence proof is still lacking, although we observed convergence of the critical values for a particular ratio of Δt to $\Delta\Gamma$ when roundoff error amplification was controlled. Clearly the model studied in this paper cannot describe all aspects of a real mixing layer. However, it appears that a periodic vortex sheet with analytic perturbations is capable of modelling some features of the initial stages of transition in turbulent mixing layers. In the future we hope to restore some of the physical effects neglected by this model in order to facilitate comparison with experiments.

N	k_b	$t_c^N\,(5 \le k \le k_b)$	$\mu_c^N\,(1 \le k \le 15)$
50	20	0·5	0·736
100	40	0·46	1·11
124	50	0·448	1·226
166	70	0·432	1·366
200	90	0·425	1·446
250	115	0·416	1·531
312	140	0·4096	1·606
400	180	0·4025	1·675
∞	----	0·38	1·9

TABLE 2.1

Least squares estimates for the critical values t_c^N, μ_c^N for various values of N. Note the different ranges fit to obtain columns 3 and 4. The extrapolated values t_c^∞, μ_c^∞ in the last row were obtained by fitting a quadratic function through the eight data points as in figure 2.3 .

N \ α	0·0025	0·005	0·01	0·02	0·04	0·08
50	0·88	0·68	0·50	0·34	0·22	0·12
100	0·80	0·62	0·46	0·31	0·19	0·12
200	0·75	0·58	0·425	0·285	0·175	0·12
250	0·74	0·572	0·416	0·28	0·172	0·116
∞	0·69	0·53	0·38	0·25	0·16	0·11

TABLE 4.1a

Values of t_c^N for various α and N using initial condition (4.1). The row labelled ∞ was obtained by least squares fitting of the four values for fixed α.

N \ α	0·0025	0·005	0·01	0·02	0·04	0·08
50	1·14	0·98	0·84	0·66	0·5	0·36
100	1·08	0·93	0·77	0·61	0·45	0·31
200	1·045	0·89	0·73	0·57	0·42	0·285
250	1·036	0·876	0·716	0·56	0·412	0·28
∞	1·00	0·83	0·68	0·52	0·38	0·26

TABLE 4.1b

Same as above except that initial condition (4.2) was used.

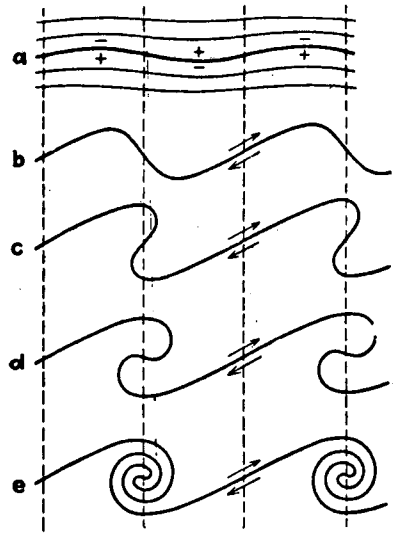

FIG. 165*a–e*.—Instability of a surface of separation.

Figure 0.1 Roll up of a vortex sheet. (Prandtl & Tietjens 1934)

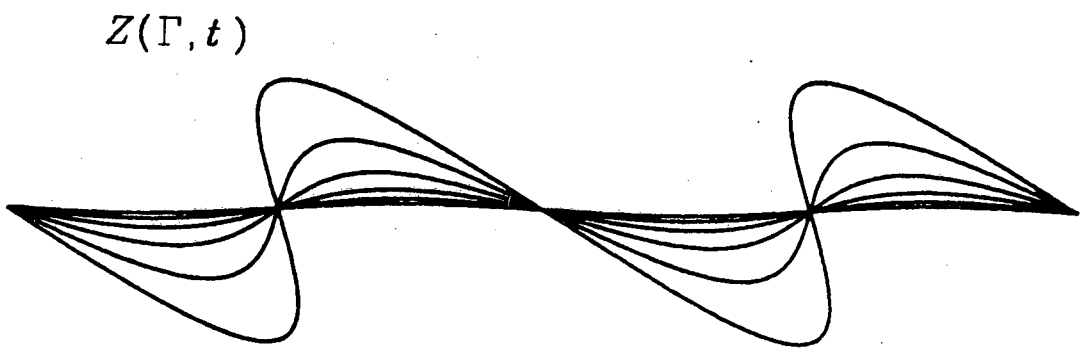

Figure 0.2 Plots of the linear theory growing mode (0.3a) with $a = 0{\cdot}01$ for $t = 0\,,\ 0{\cdot}1\,,\ 0{\cdot}2\,,\ 0{\cdot}3\,,\ 0{\cdot}4\,,\ 0{\cdot}5\,.$

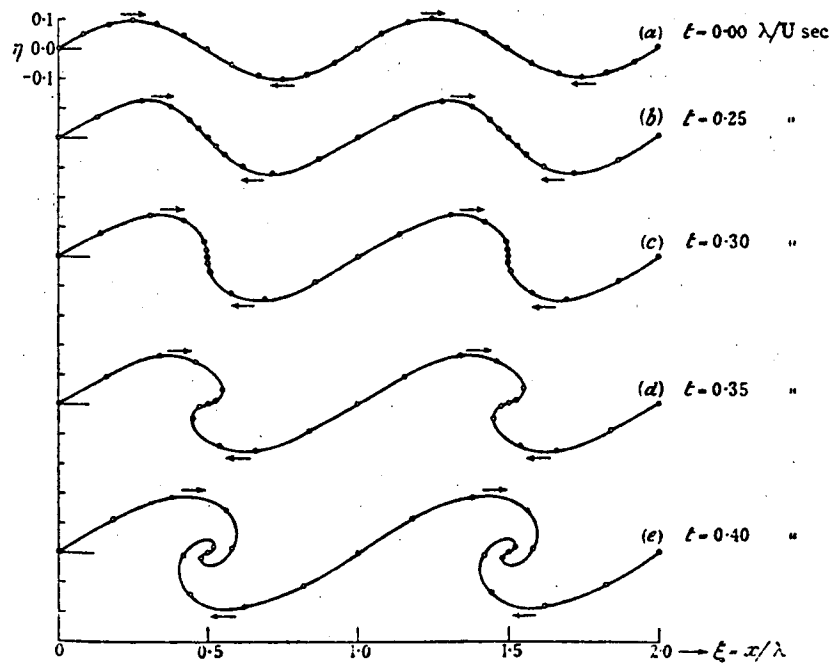

FIG. 4.

Figure 0.3 Rosenhead's (1931) solution of equations (0.4) by Euler's method with $N = 12$ and $\Delta t = 0{\cdot}05$.

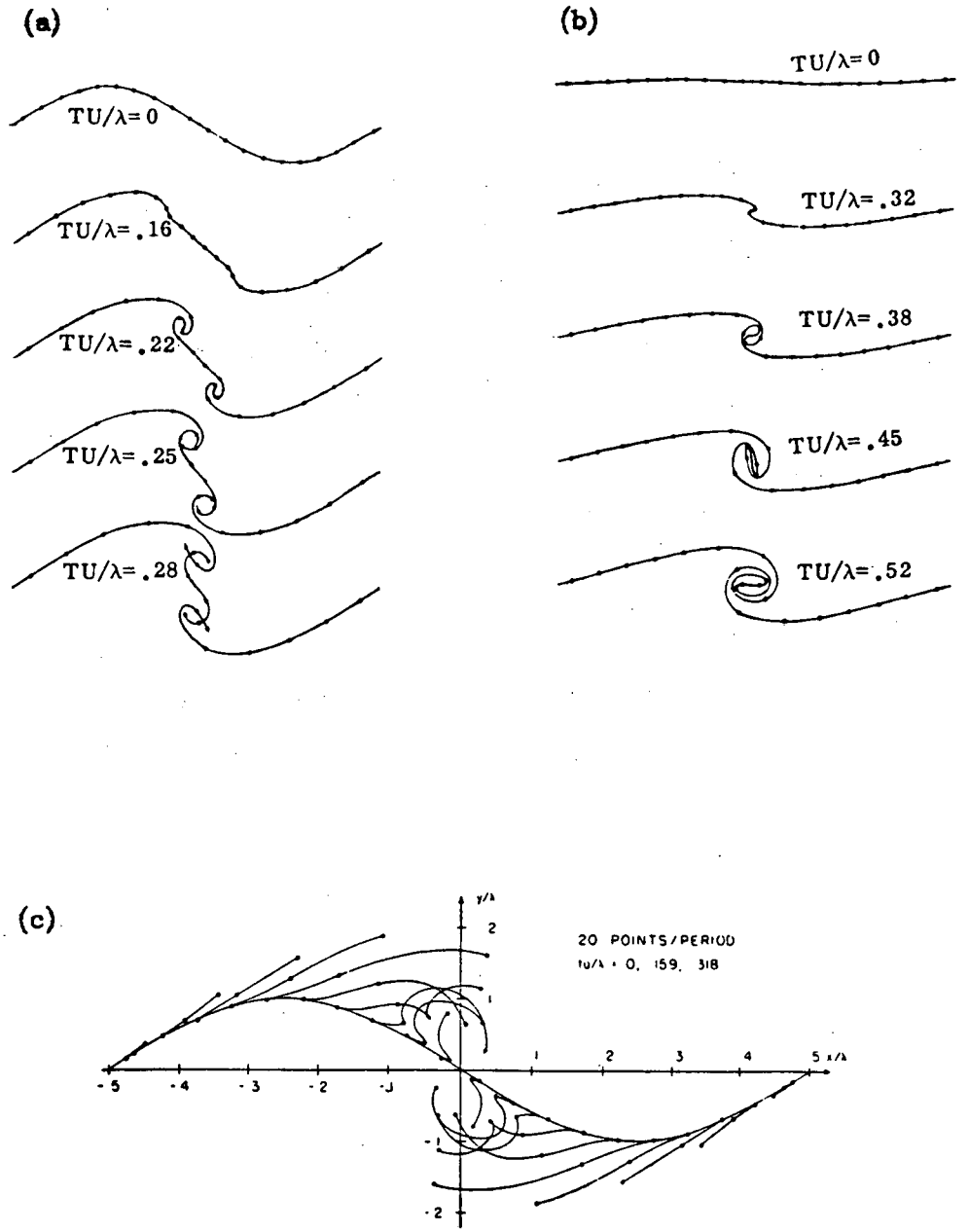

Figure 0.4 Numerical solution of equations (0.4) with $N = 20$ and Δt in the range 0·0005 -0·002 using 4th order Runge-Kutta integration.

(a) large initial amplitude (b) small initial amplitude (c) vortex trajectories for initial conditions similar to (b) (copied from Birkhoff (1962) and Birkhoff & Fisher (1959))

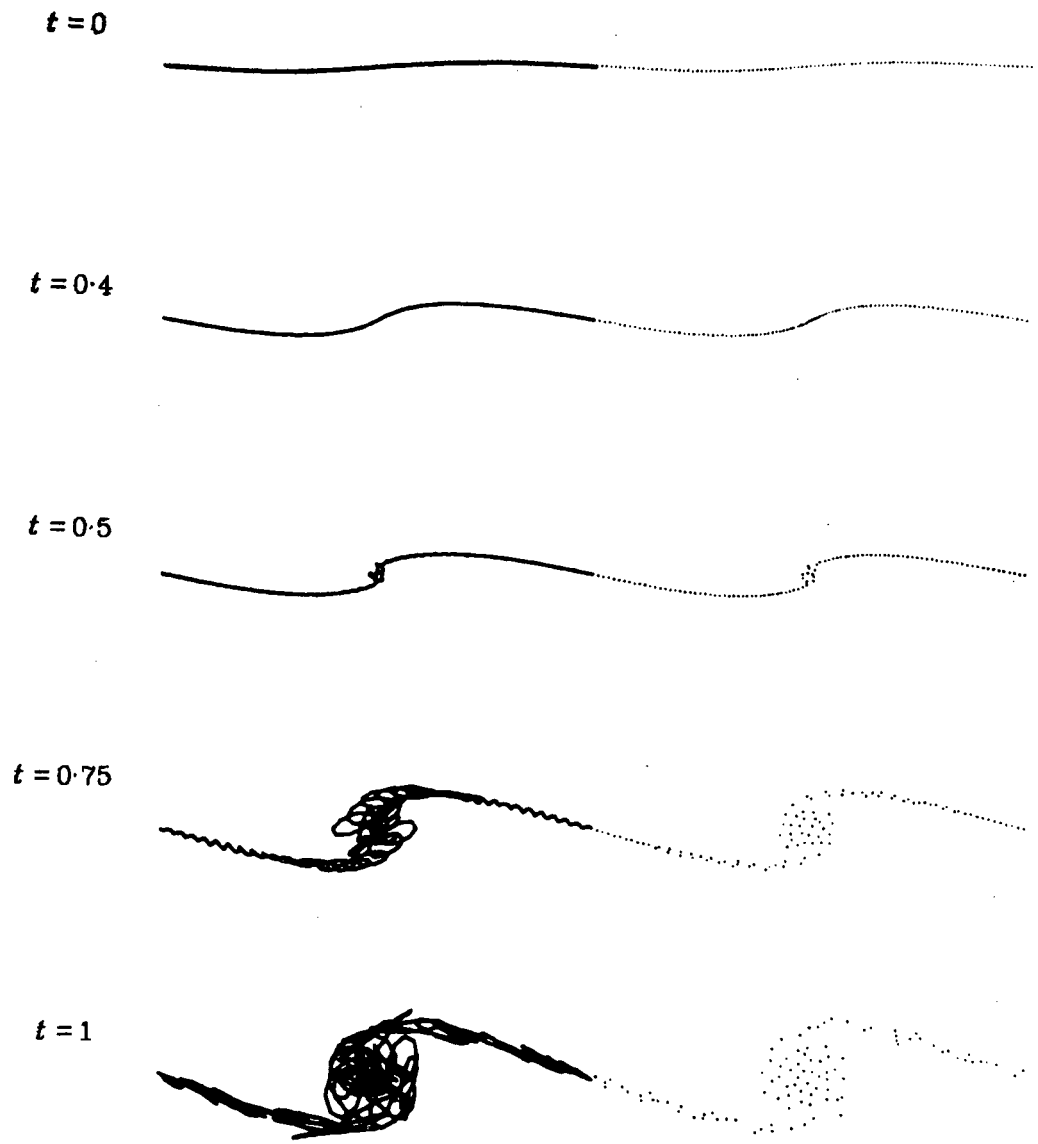

Figure 1.1 Solution of equations (0.4) with $N = 100$ by Euler's method using $\Delta t = 0{\cdot}01$. The initial condition is (0.3a) with $a = 0{\cdot}01$ and $t = 0$. Point vortex positions are on the right and the trigonometric interpolating curve is drawn on the left. This computation used 14 digits of precision.

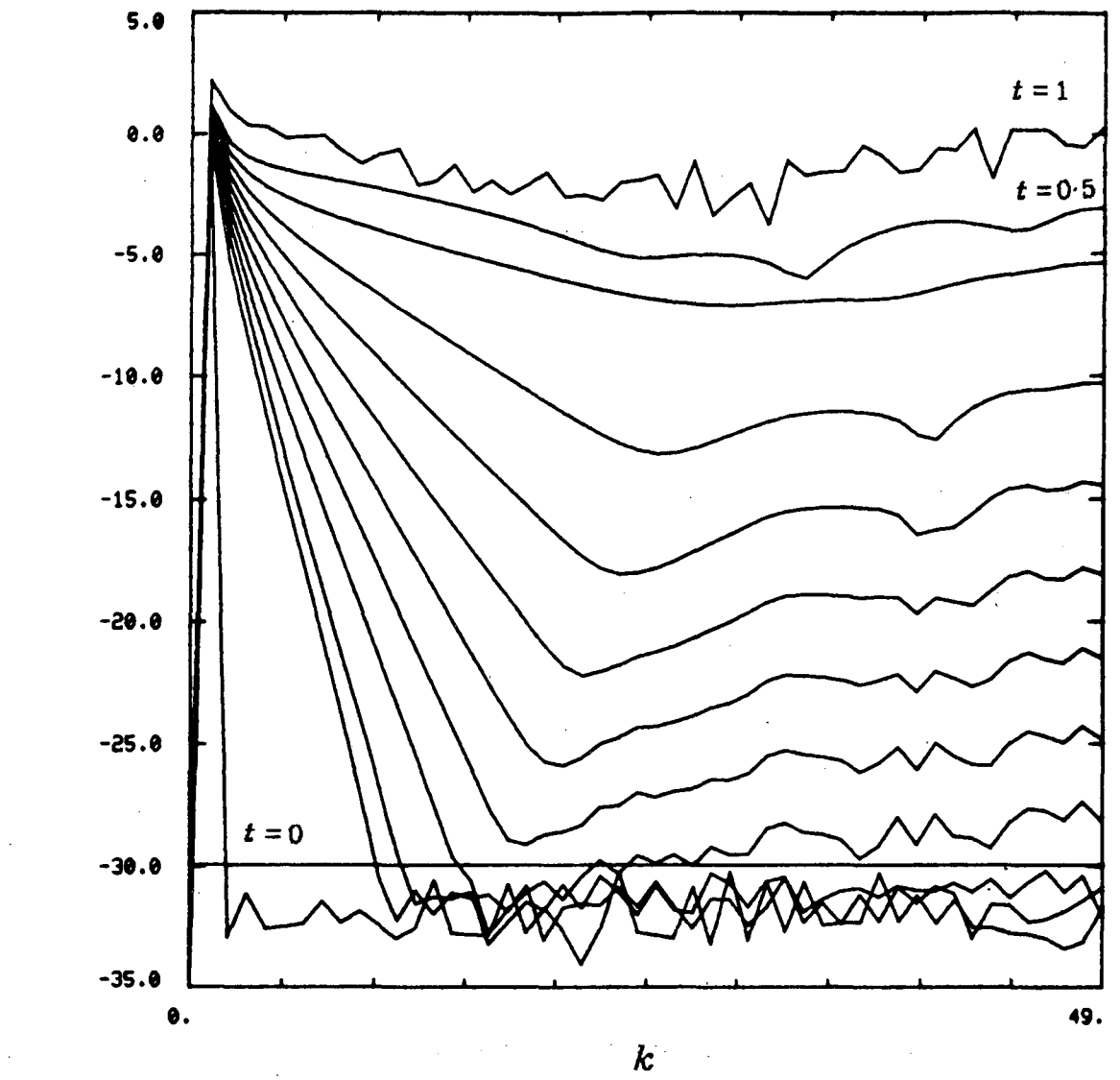

Figure 1.2 A linear-log plot of the discrete Fourier coefficient amplitudes of the perturbation, $P(\Gamma, t)$ for the solution in figure 1.1 at time intervals of 0·05 between $t = 0$ and $t = 0{\cdot}5$ and at $t = 1$.

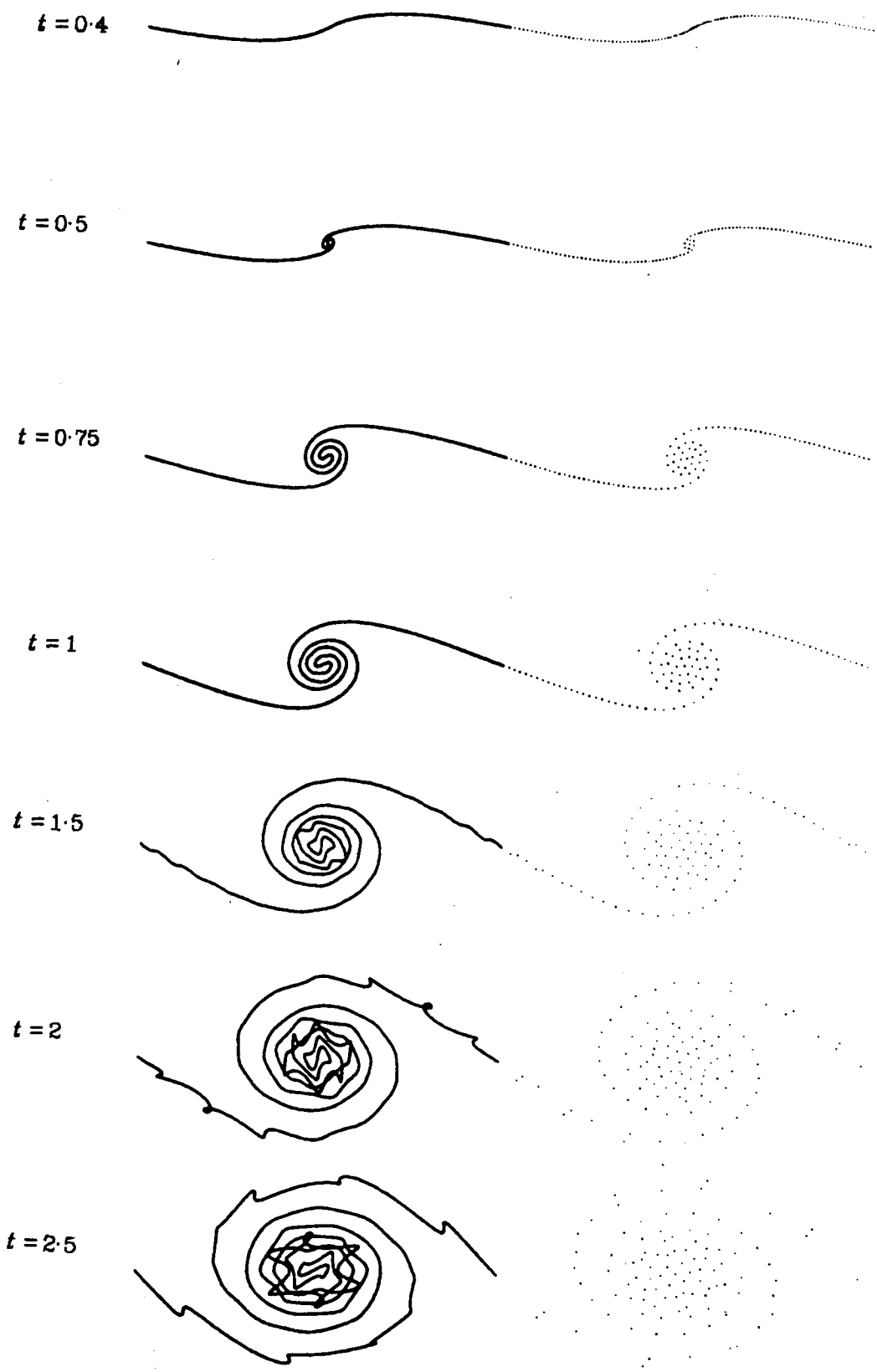

Figure 1.3 Same parameters as figure 1.1 except with the chopping procedure turned on.

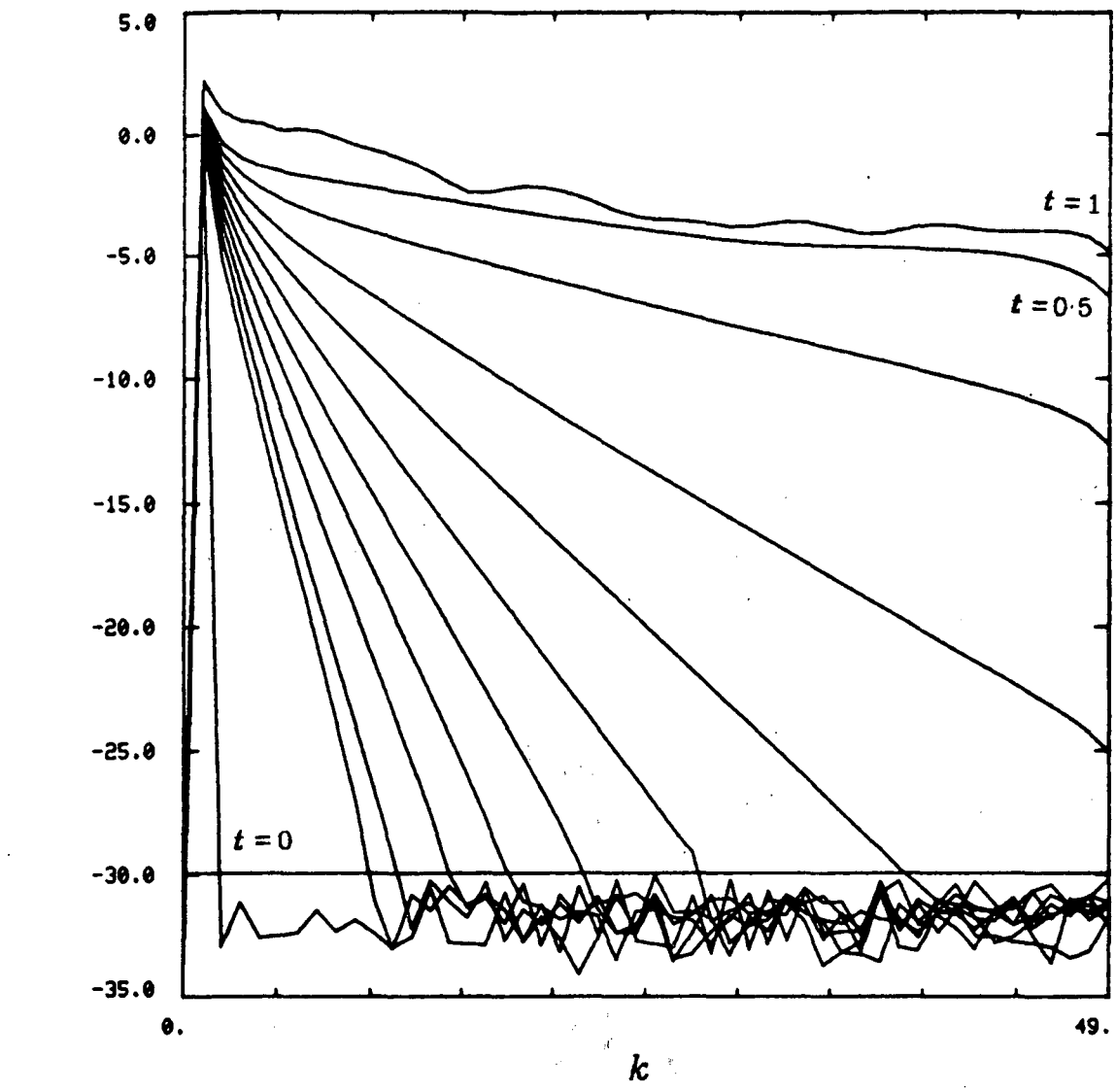

Figure 1.4a A linear-log plot of the discrete Fourier coefficient amplitudes of the perturbation, $P(\Gamma, t)$ for the solution in figure 1.3 at time intervals of 0·05 between $t = 0$ and $t = 0{\cdot}5$ and at $t = 1$.

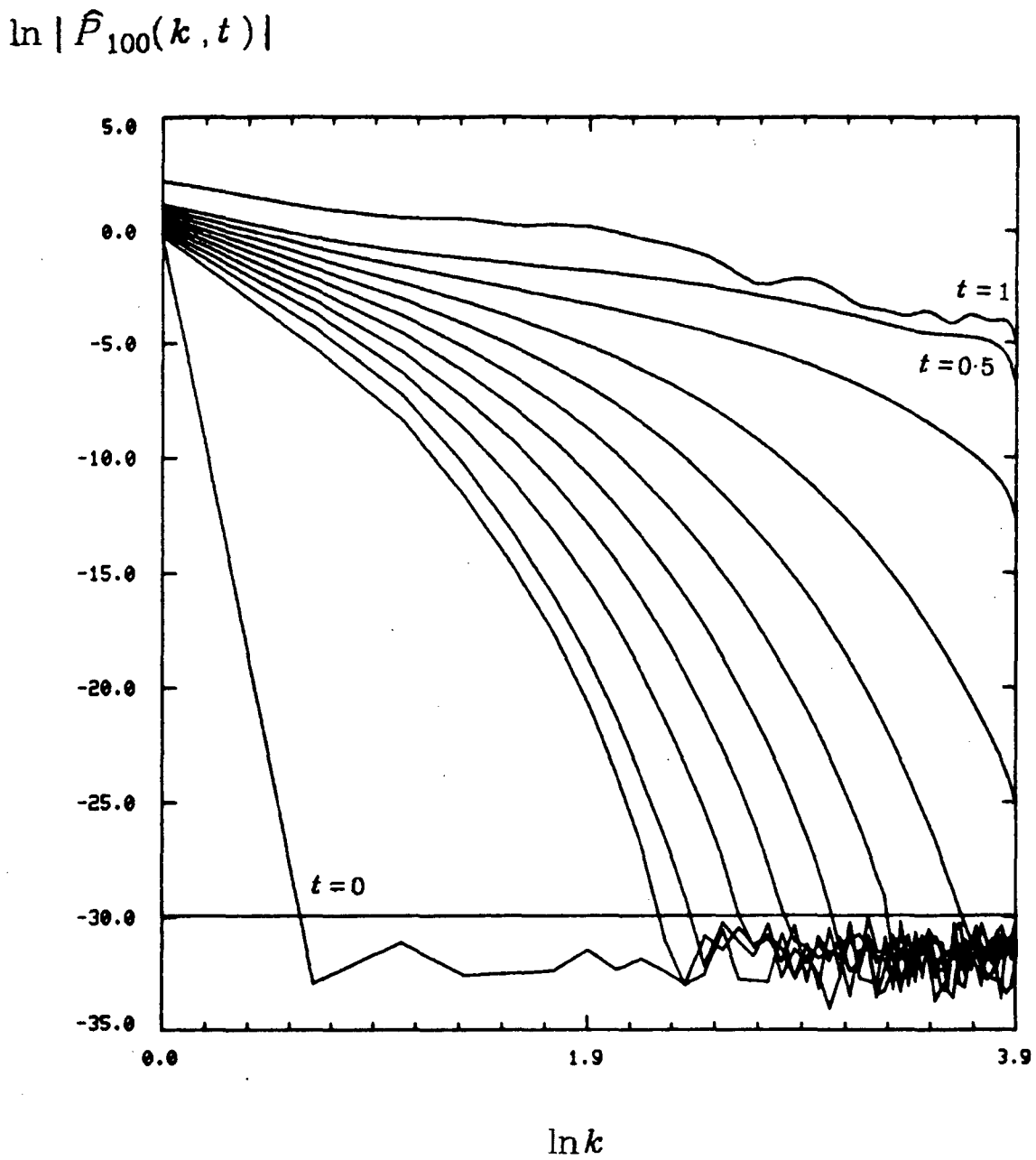

Figure 1.4b A log-log plot of the discrete Fourier coefficient amplitudes of the perturbation, $P(\Gamma, t)$ for the solution in figure 1.3 at time intervals of 0·05 between $t = 0$ and $t = 0{\cdot}5$ and at $t = 1$.

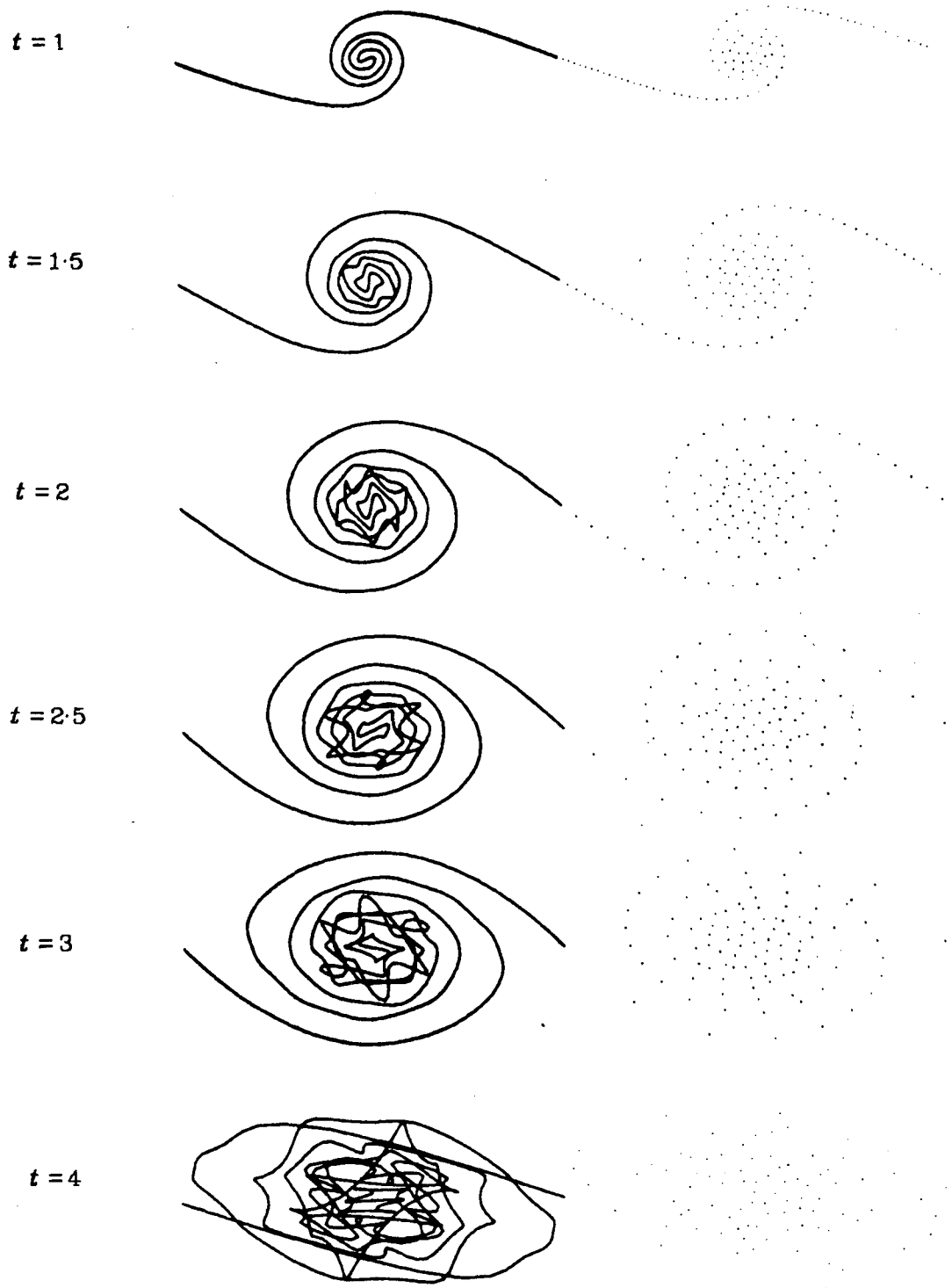

Figure 1.5 Same parameters as figure 1.1 except with 29 digits of accuracy and the chopping procedure turned off.

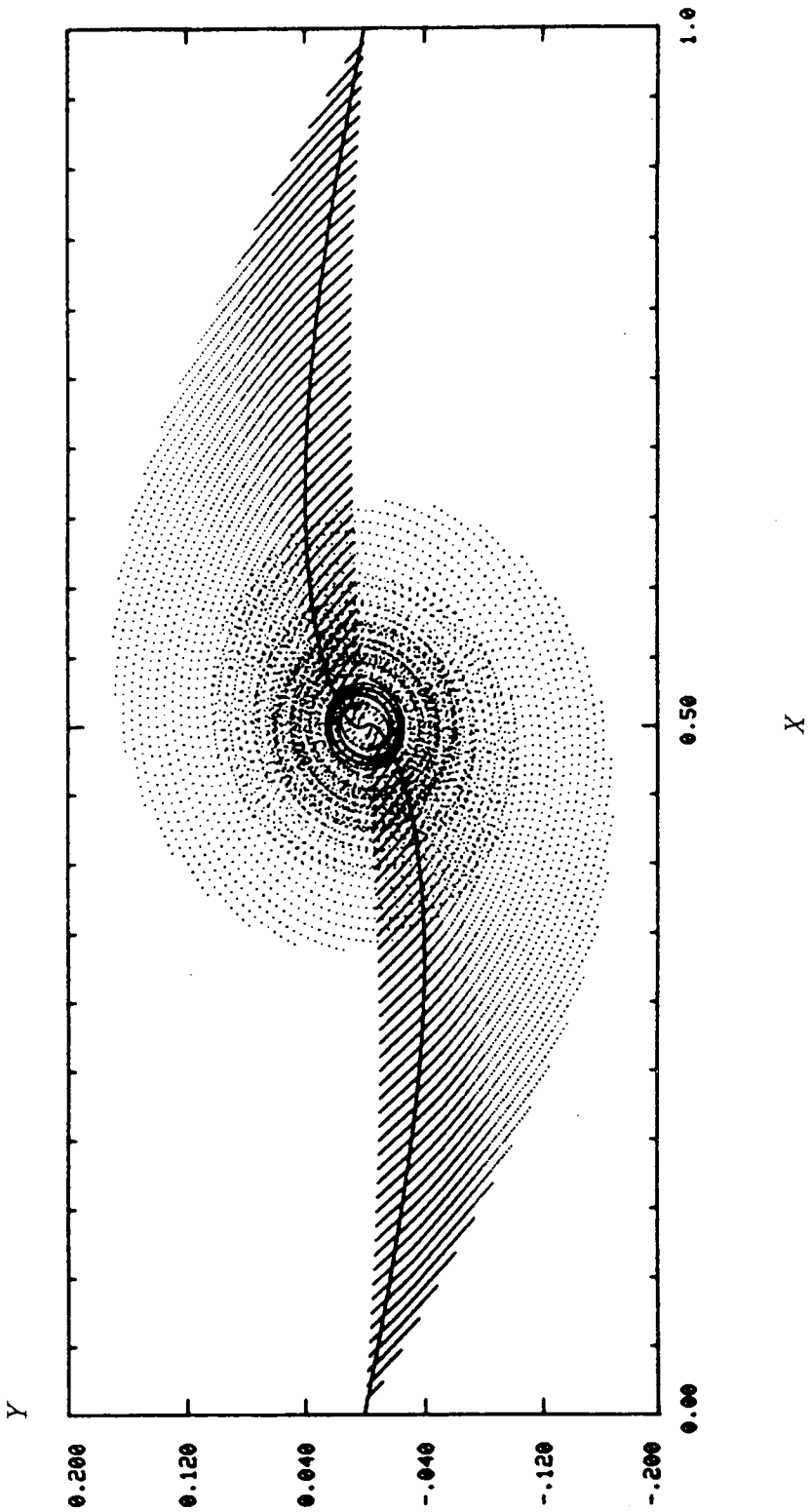

Figure 1.6 Point vortex trajectories for figure 1.5 up to $t = 1.5$. The solid line shows the interpolating curve at $t = 0{\cdot}46$, when the sheet begins to roll up.

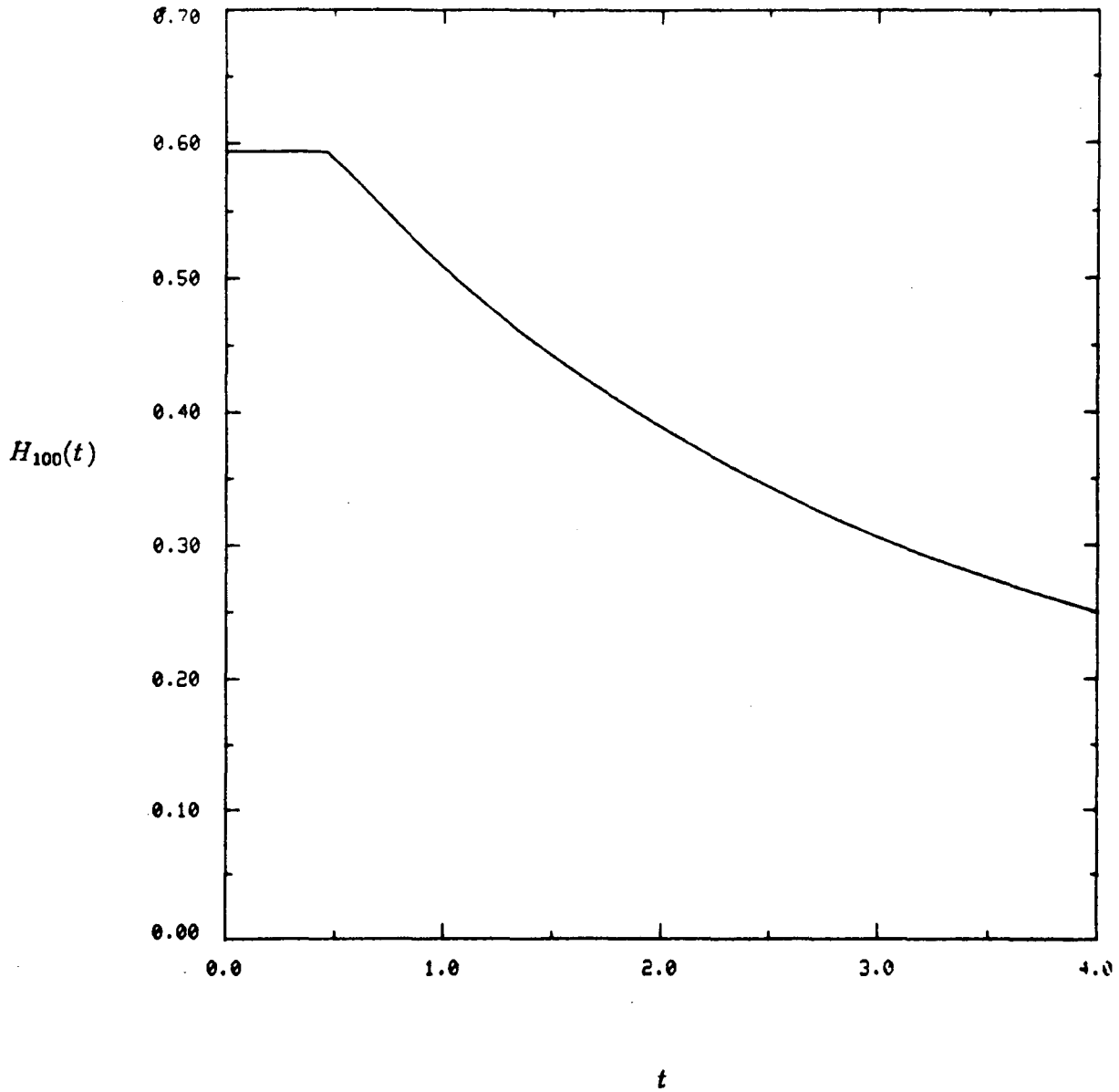

Figure 1.7 A plot of the Hamiltonian, $H_{100}(t)$ vs. time for the results shown in figure 1.5 .

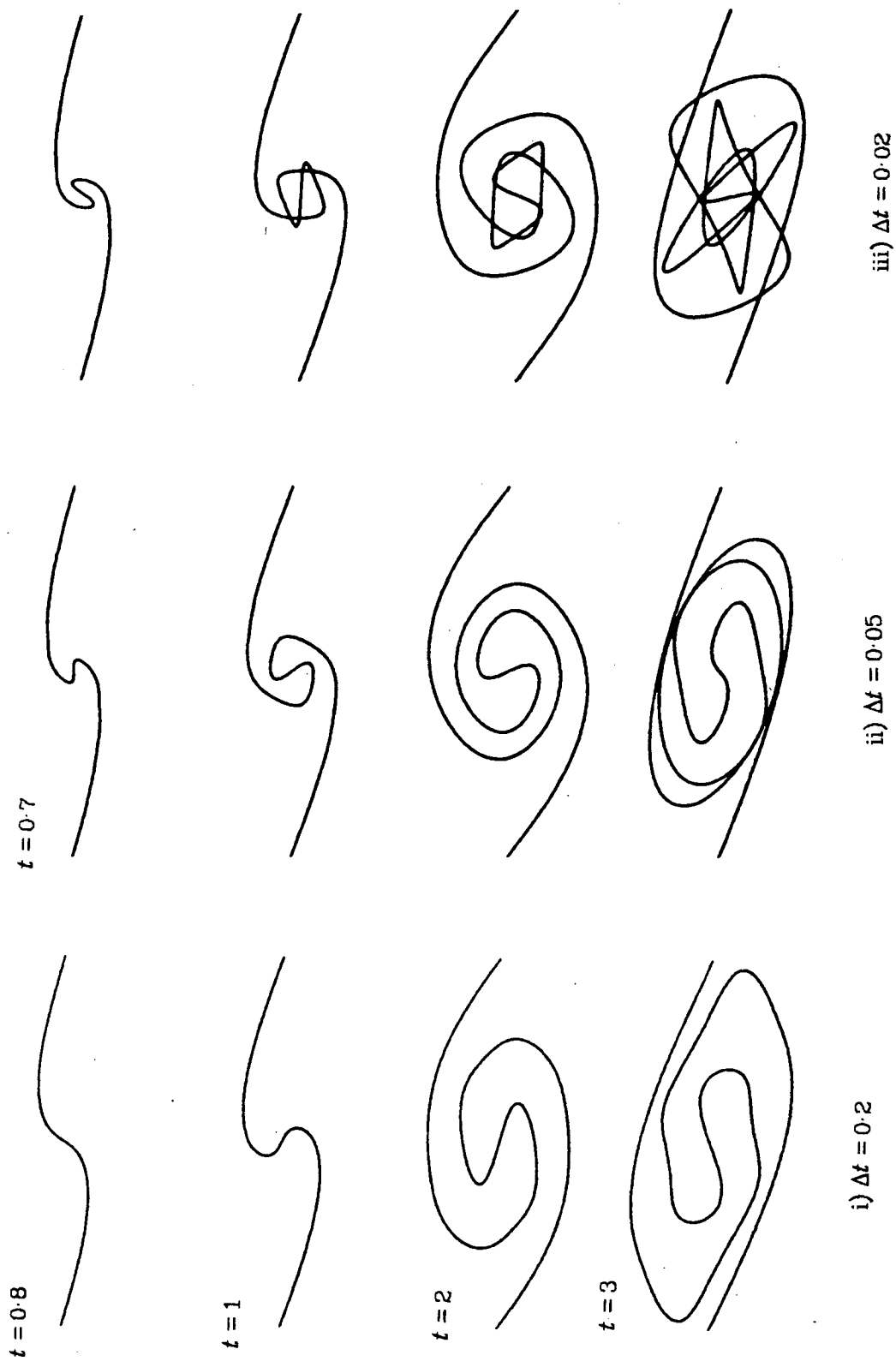

Figure 1.8a Evolution with $N = 20$ using Euler's method.

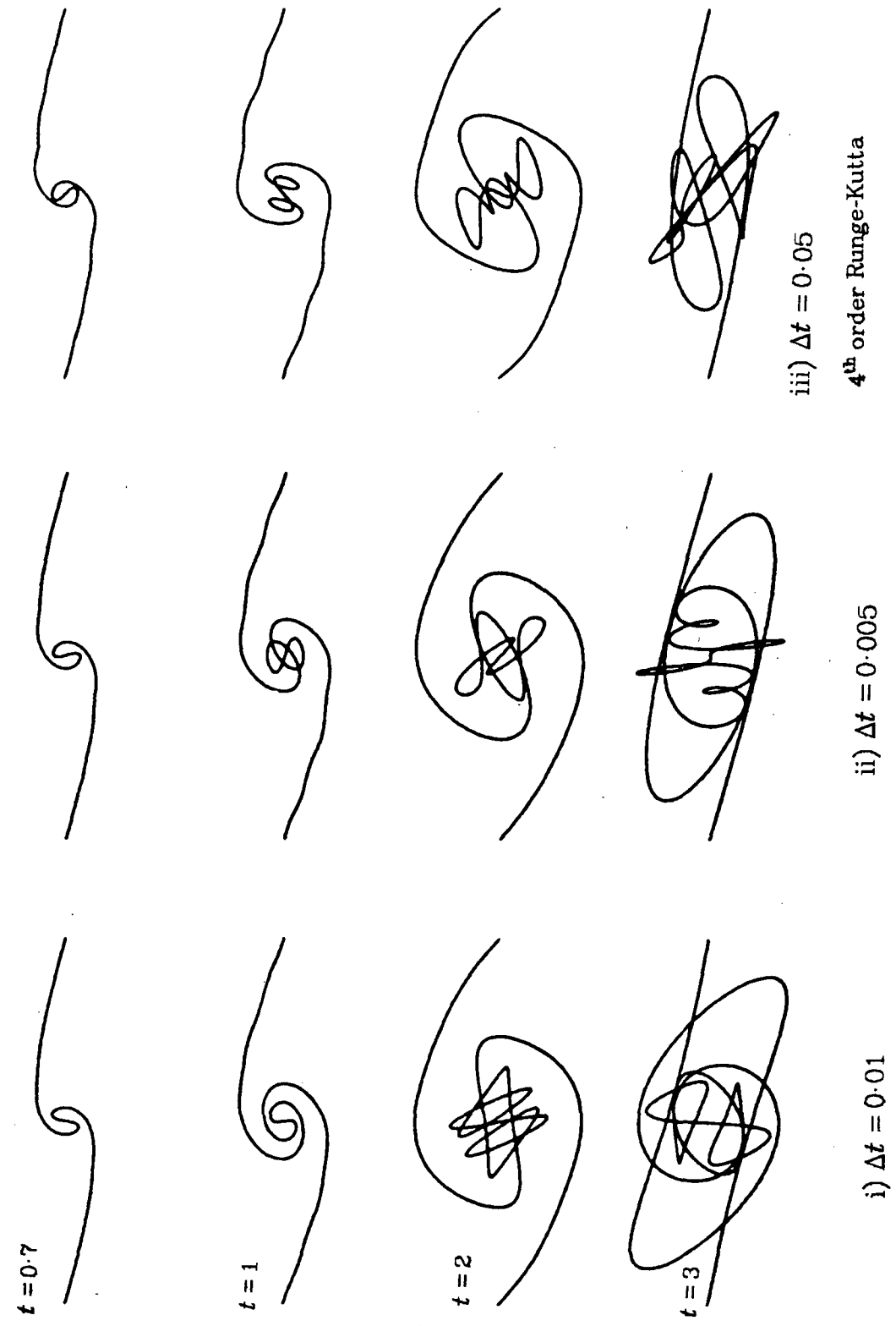

Figure 1.8b Evolution with $N = 20$ using Euler's method for i) , ii) and 4^{th} order Runge-Kutta for iii).

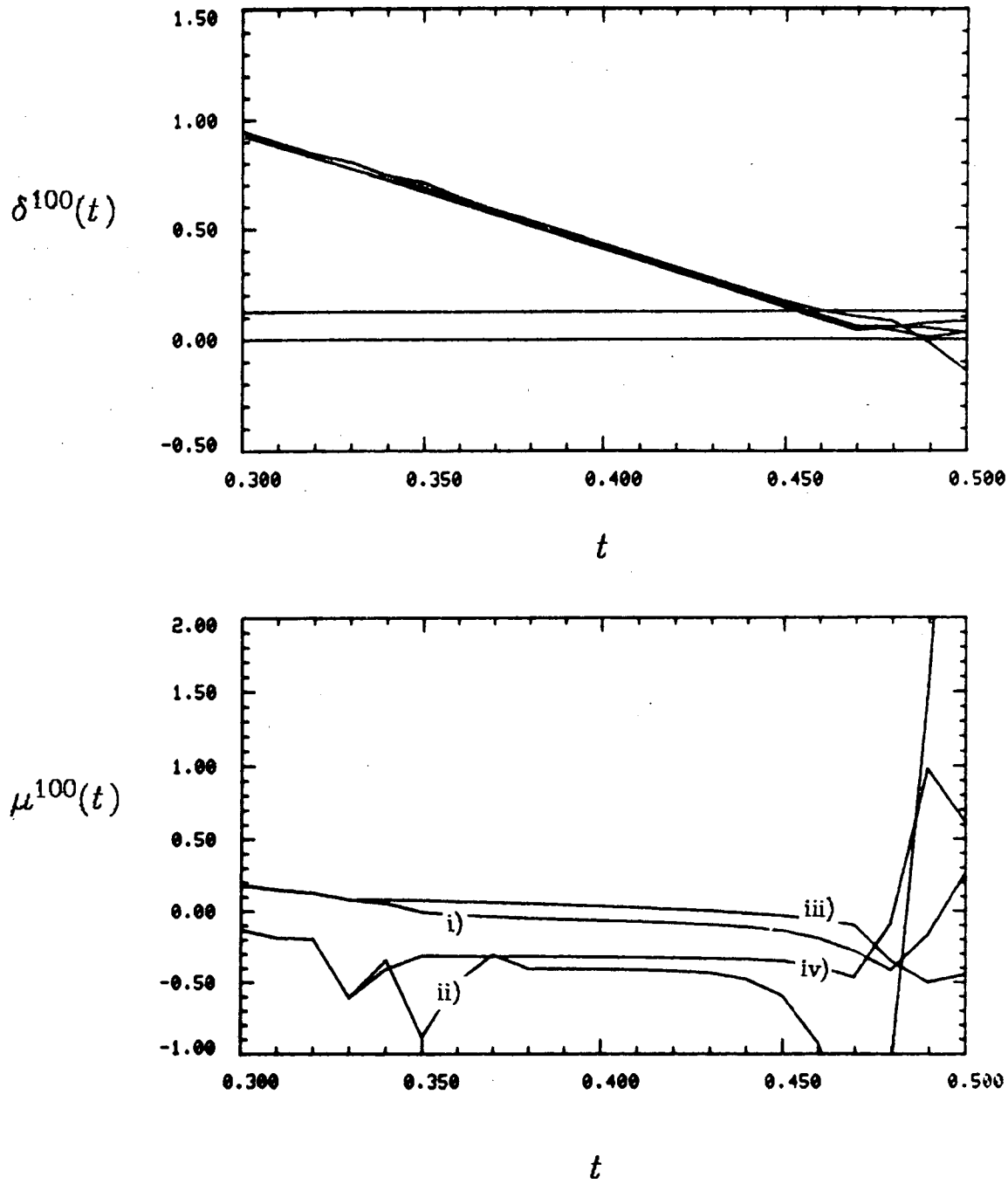

Figure 2.1 Plots of (a) $\delta^{100}(t)$ and $\mu^{100}(t)$ vs. time, determined by least squares fitting to the spectrum in figures 1.4a,b over a band of high wavenumbers:

i) $5 \le k \le 40$ ii) $20 \le k \le 40$ iii) $5 \le k \le 30$ iv) $20 \le k \le 30$.

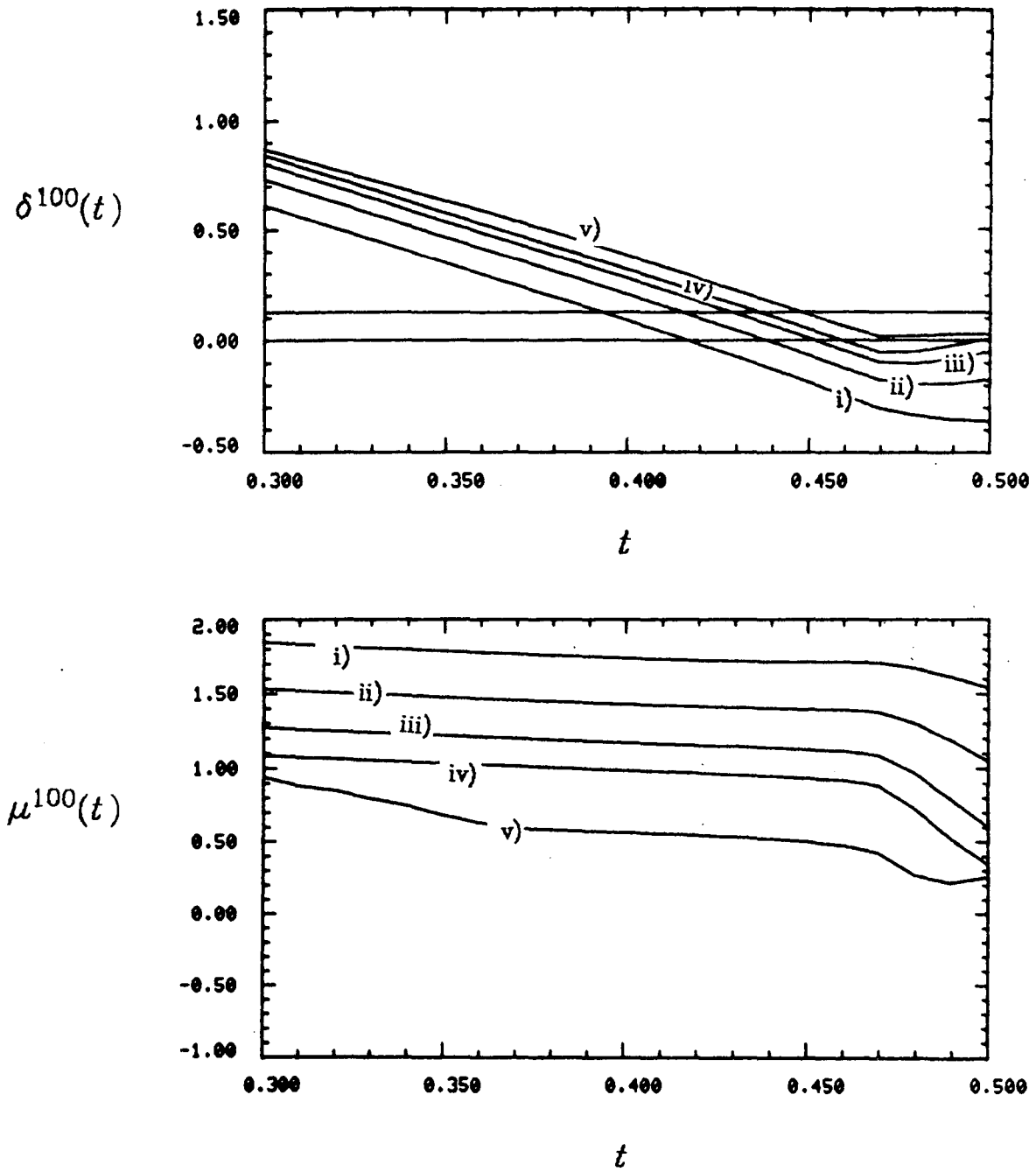

Figure 2.2 Plots of (a) $\delta^{100}(t)$ and $\mu^{100}(t)$ vs. time, determined by least squares fitting to the spectrum in figures 1.4a,b over a band of low wavenumbers:

i) $1 \le k \le 6$ ii) $1 \le k \le 10$ iii) $1 \le k \le 15$ iv) $1 \le k \le 20$ v) $1 \le k \le 40$.

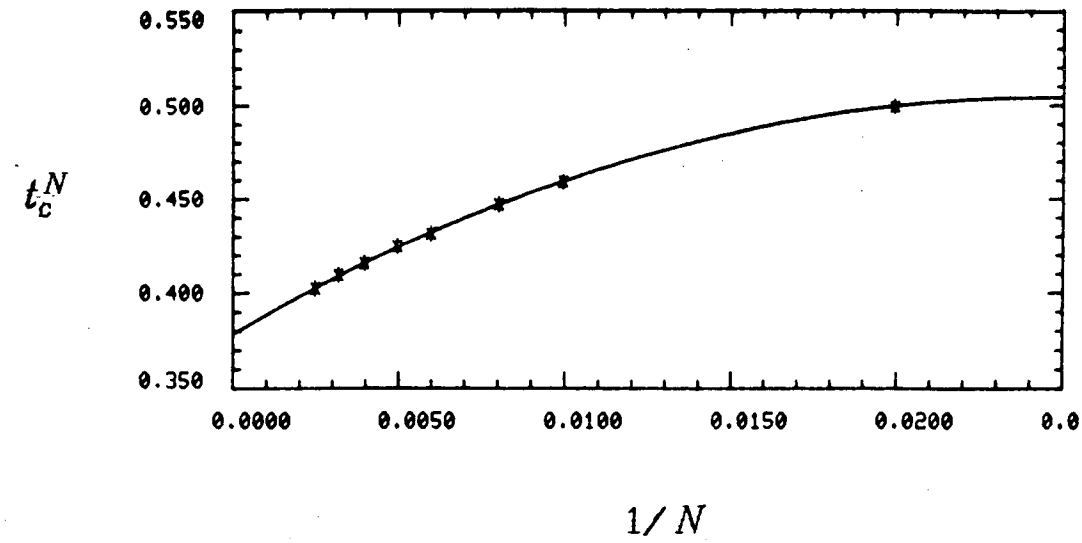

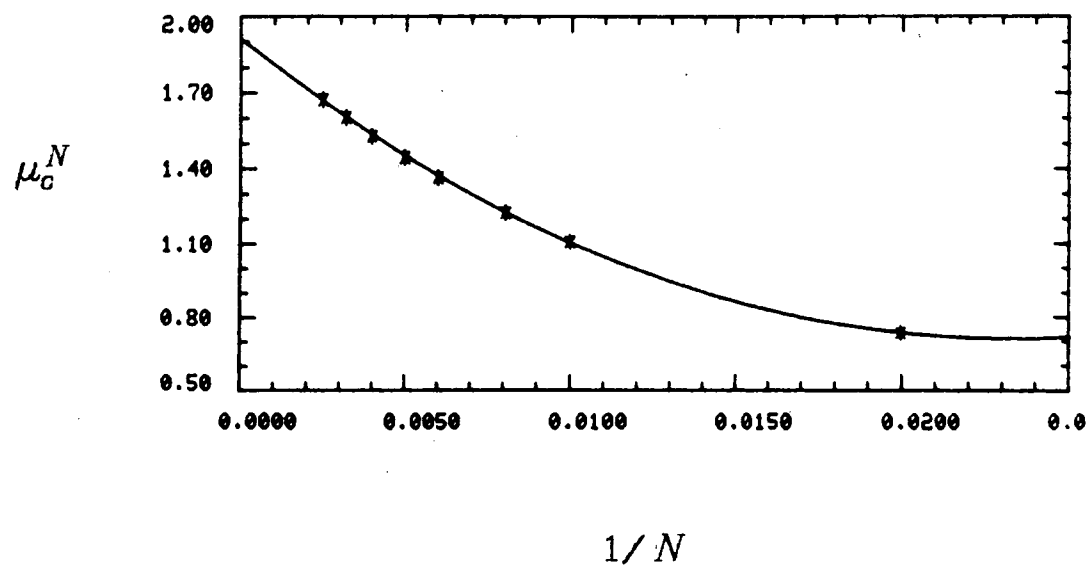

Figure 2.3 A plot of estimated values of t_c^N and μ_c^N vs. $1/N$ using Euler's method with $\Delta t = 1/N$ (Table 2.1). The curves are quadratic functons of $1/N$ whose coefficients were found by least squares fitting to the eight data points.

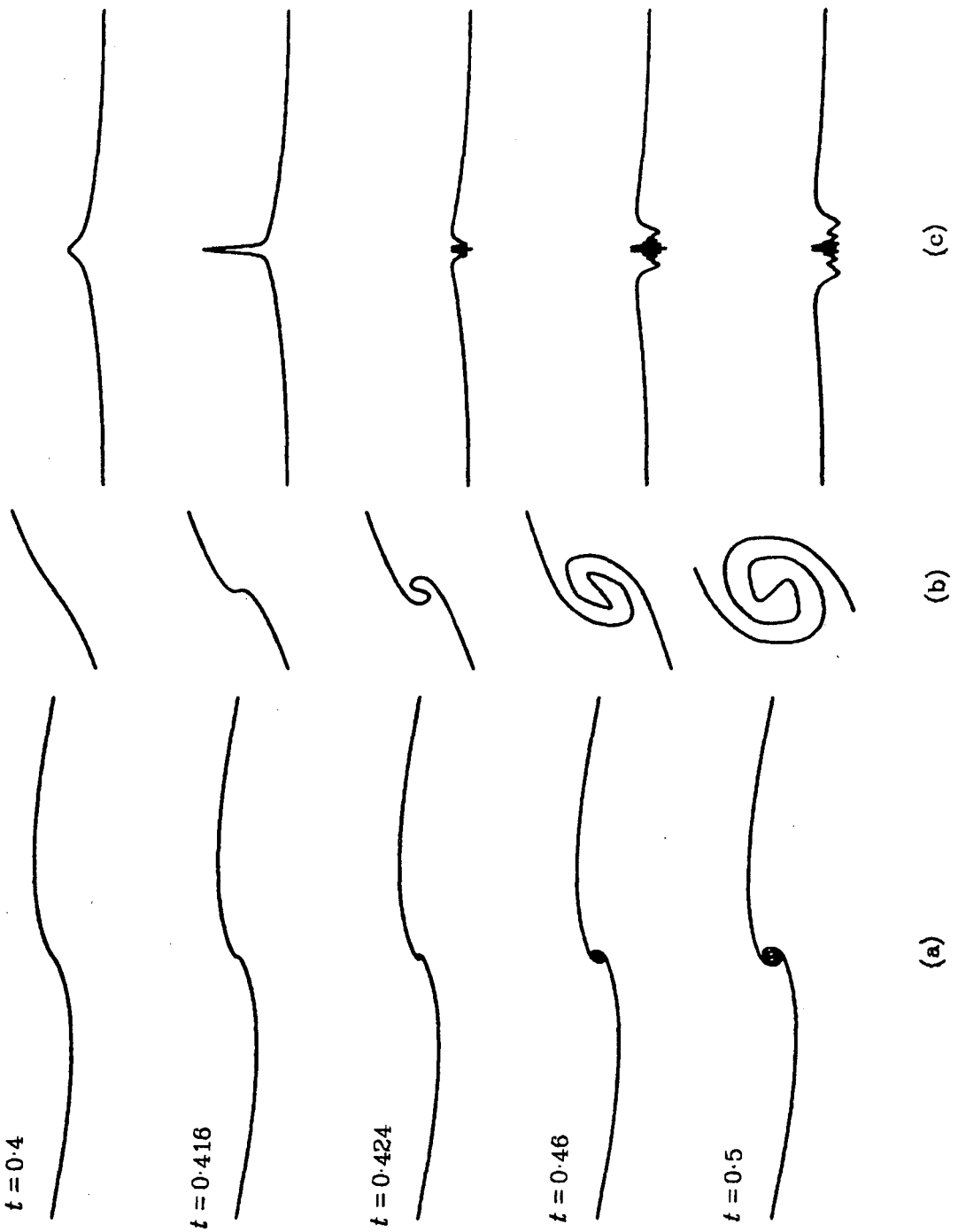

Figure 2.4 Behaviour near the critical time using $N = 250$, $\Delta t = 0{\cdot}004$ showing: (a) vortex sheet (b) closeup of the sheet in the core (c) vortex sheet strength, $\sigma(\Gamma, t)$ vs. Γ. Note that at the critical time, $t_c^{250} = 0{\cdot}416$ the vortex sheet strength has a cusp at $\Gamma = 0$ and the sheet is beginning to roll up about that point on a small scale.

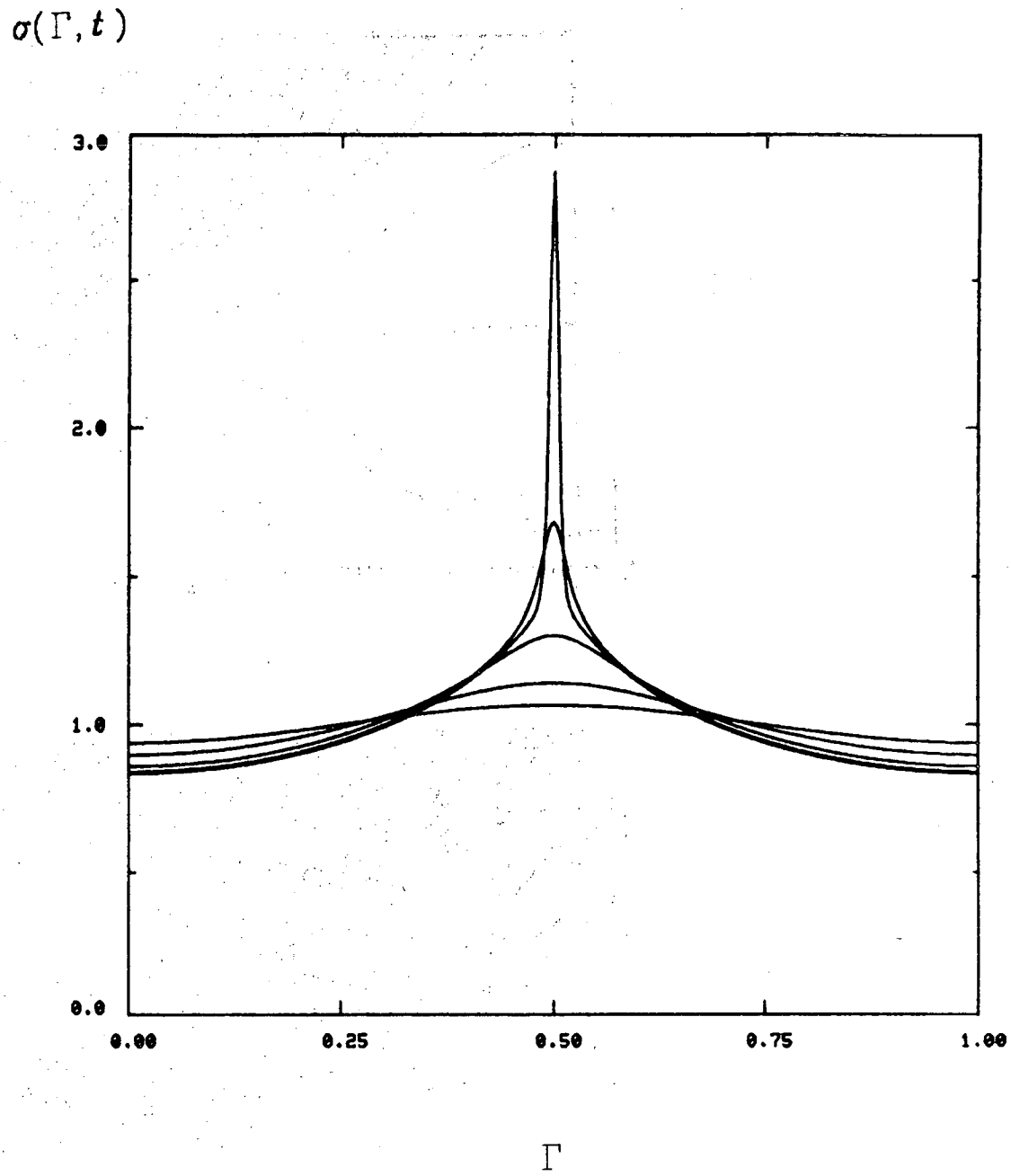

Figure 2.5 A plot of the vortex sheet strength, $\sigma(\Gamma, t)$ vs. Γ using $N = 250, \Delta t = 0{\cdot}004$. For the plotted times ($0, 0{\cdot}2, 0{\cdot}32, 0{\cdot}4, 0{\cdot}416 = t_c^{250}$), $\sigma(\Gamma = 0{\cdot}5, t)$ increases monotonically.

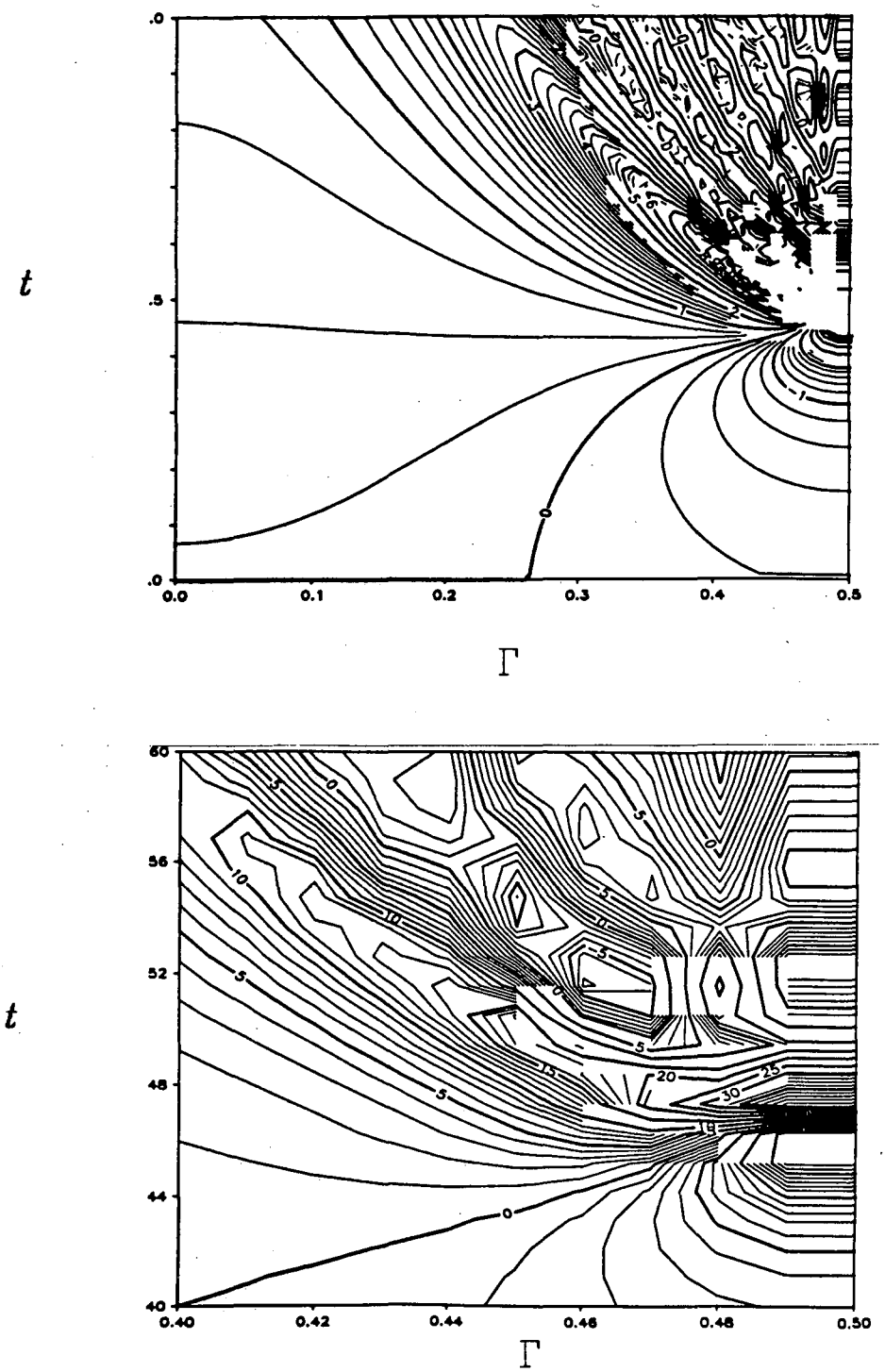

Figure 3.1 (a) A contour plot of the strain rate along the sheet, $\gamma(\Gamma, t)$ for $0 \leq \Gamma \leq 0{\cdot}5$ and $0 \leq t \leq 1$. This run used $N = 100$ and $\Delta t = 0{\cdot}01$.

(b) A closeup of figure 3.1a for $0{\cdot}4 \leq \Gamma \leq 0{\cdot}5$ and $0{\cdot}4 \leq t \leq 0{\cdot}5$. The contour lines were not smoothed.

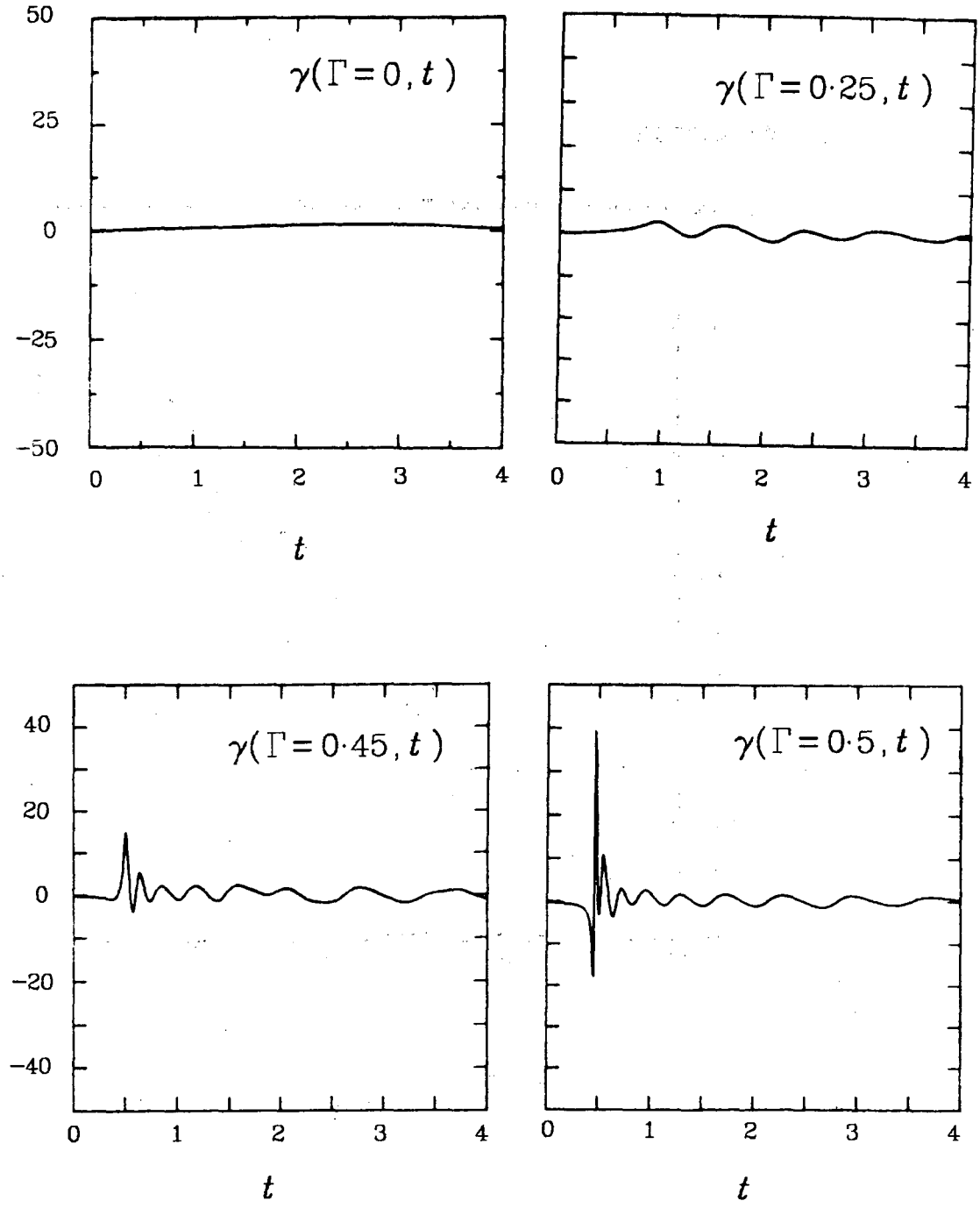

Figure 3.2 Plots of strain rate along the sheet, $\gamma(\Gamma,t)$ vs. time.

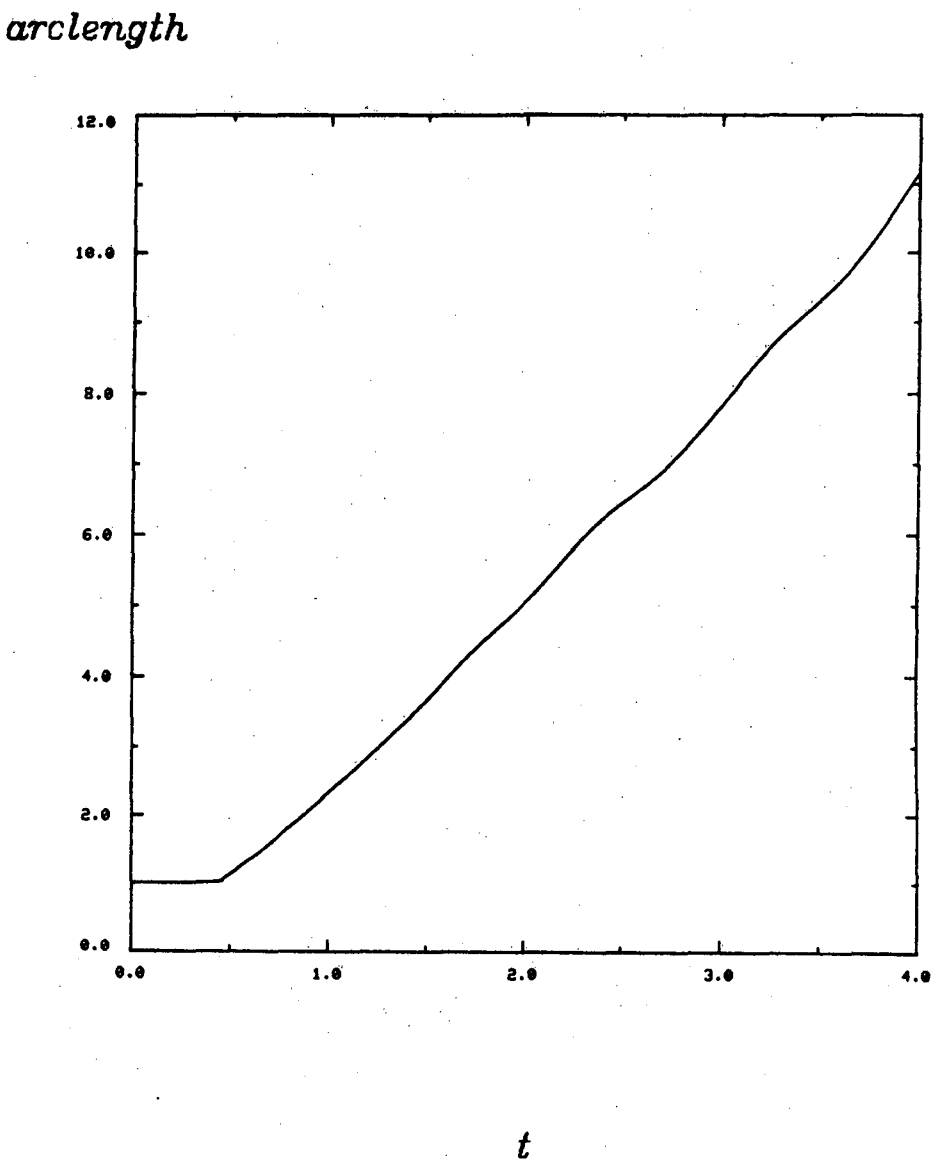

Figure 3.3 Arclength vs. time for figure 1.5 ($N = 100$). Note the approximately linear increase in arclength past $t_c^{100} = 0{\cdot}46$.

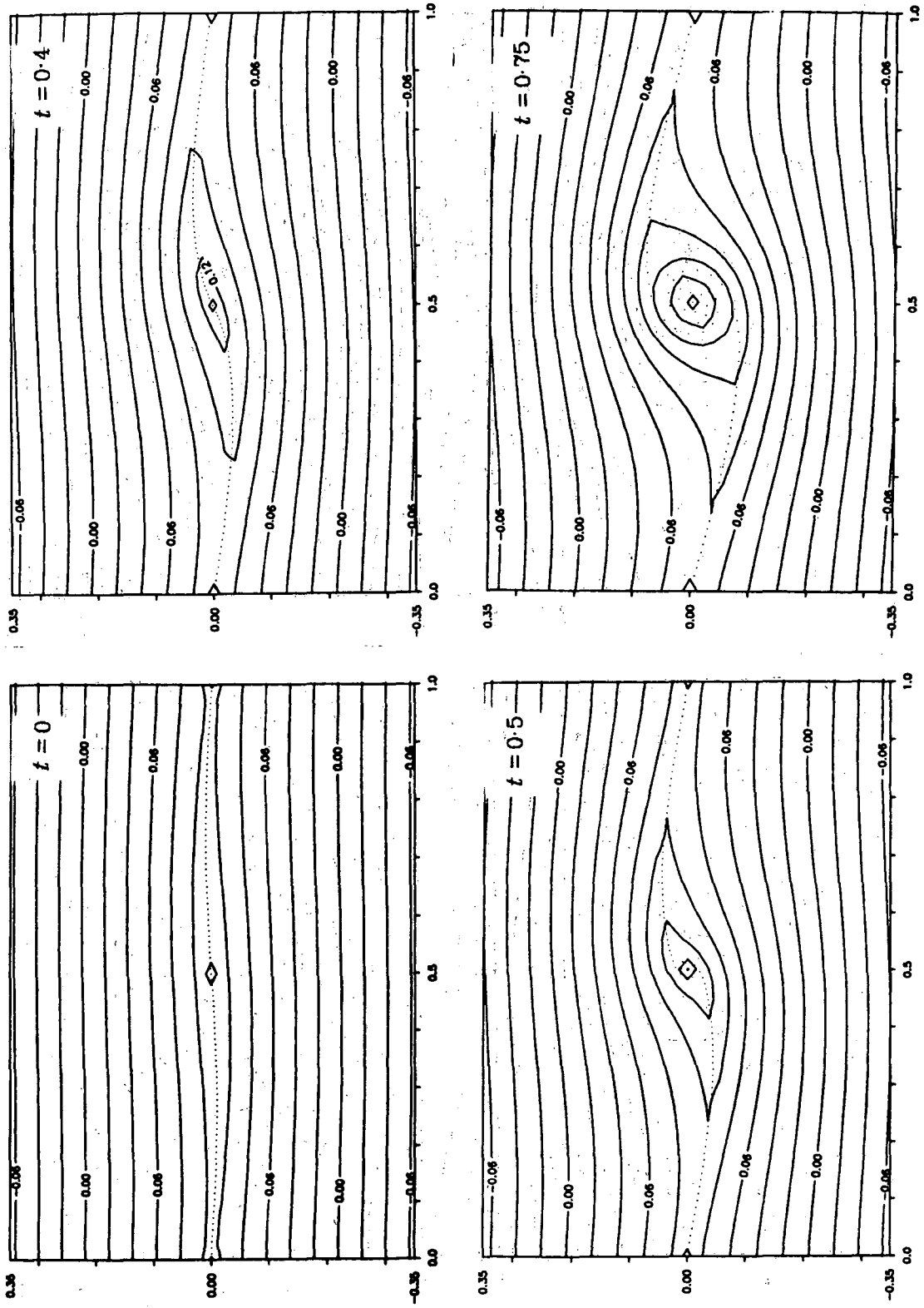

Figure 3.4 Streamline plots. The contour lines were not smoothed.

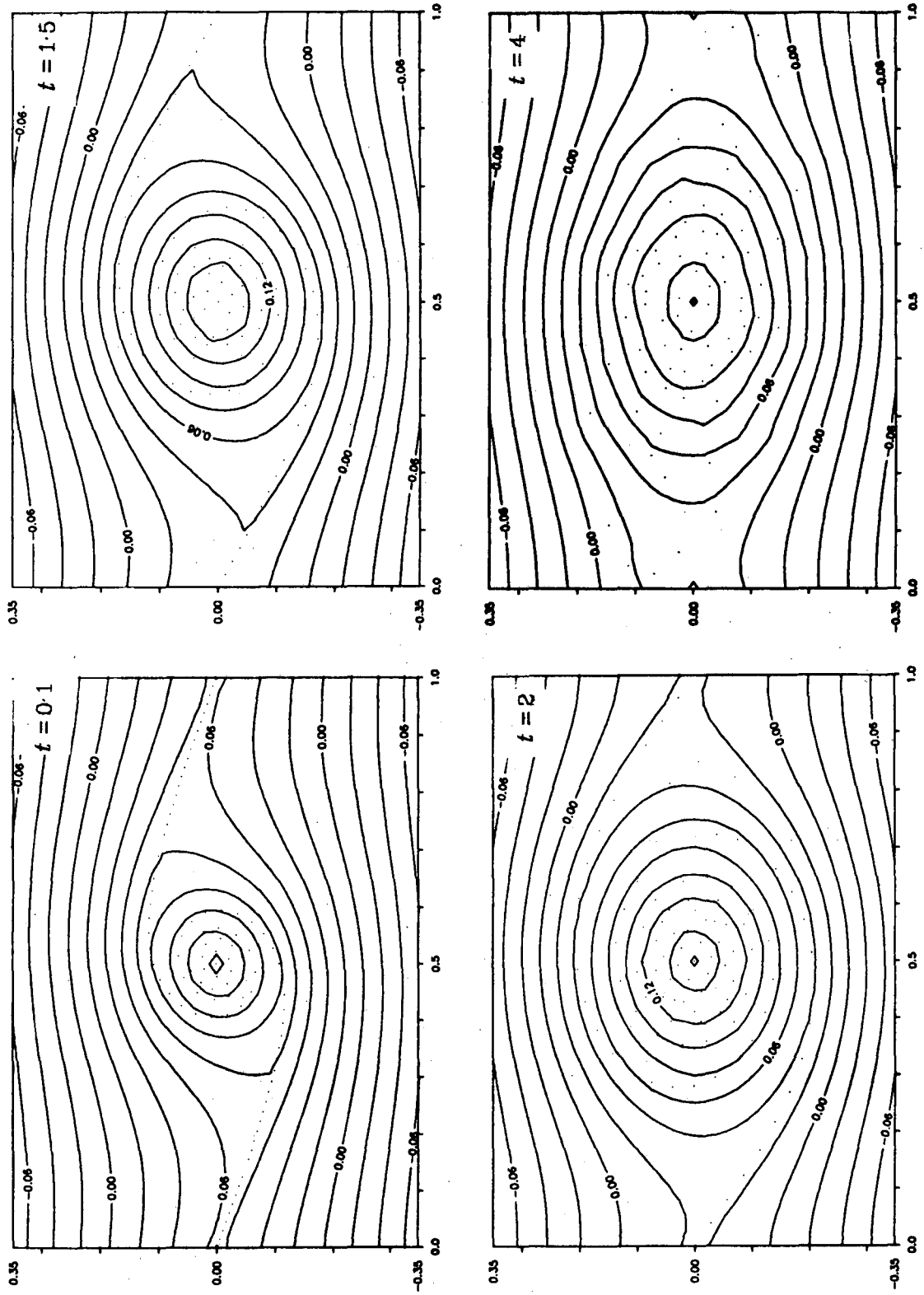

Figure 3.4 continued

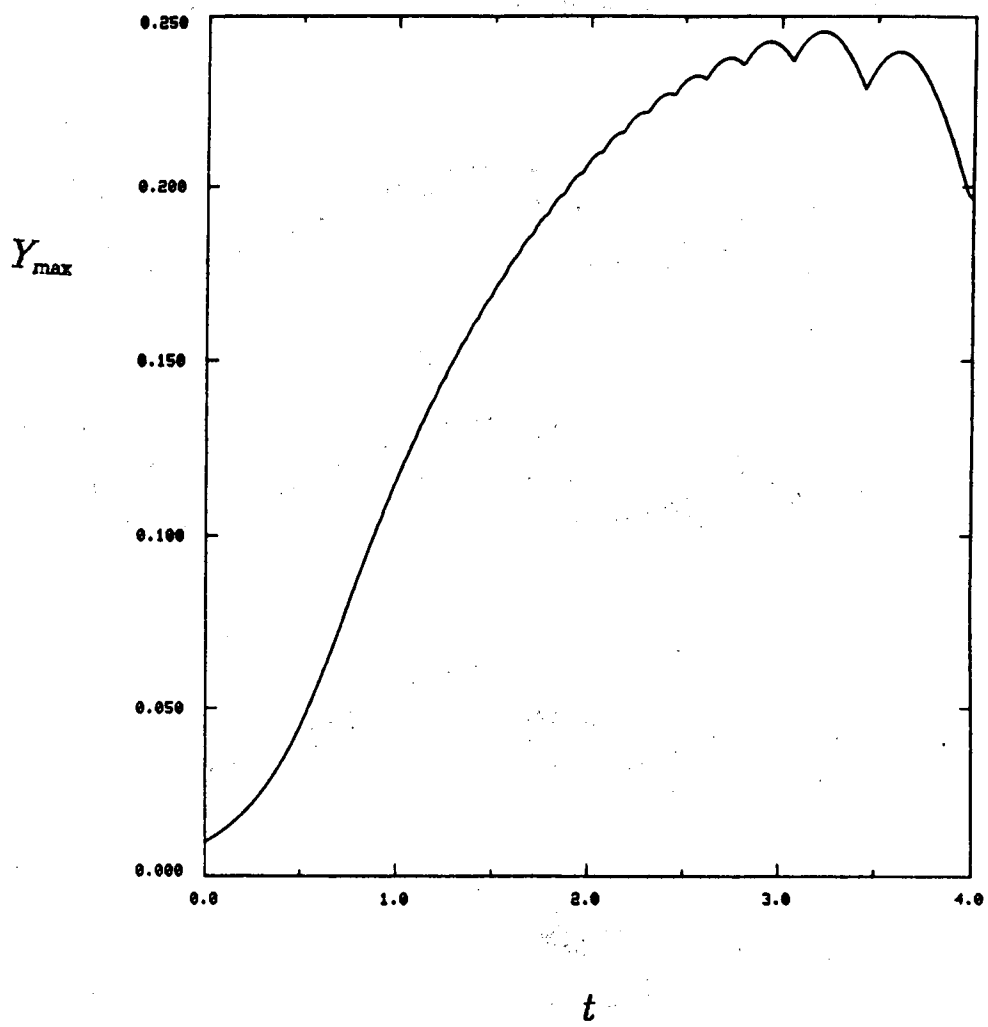

Figure 3.5 A plot of the maximum sheet amplitude, $Y_{max}(t)$ vs. time for the evolution shown in figure 1.5 .

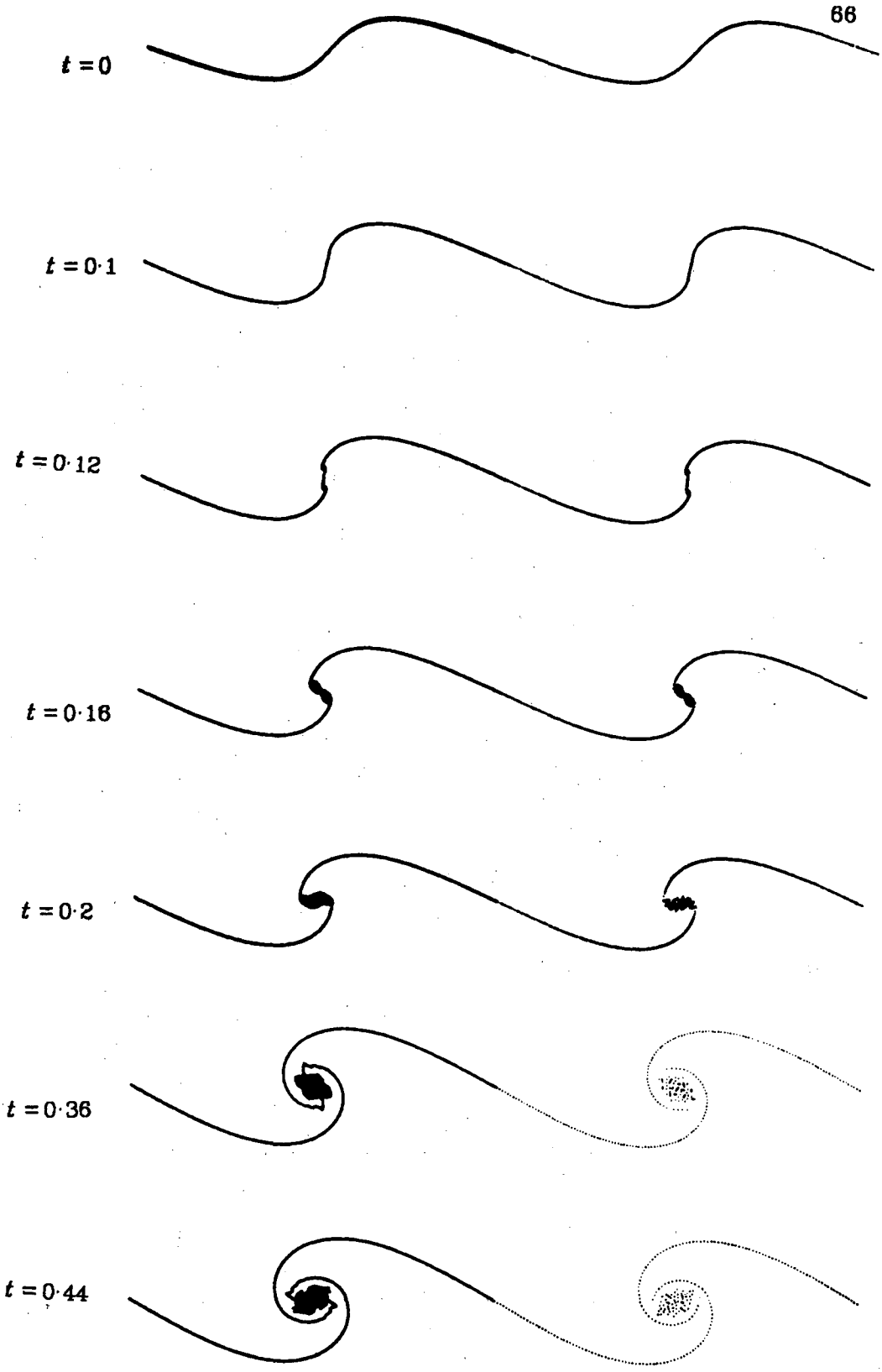

Figure 4.1 Initial condition (4.1) with $a = 0{\cdot}08$, $N = 250$ and $\Delta t = 0{\cdot}004$.

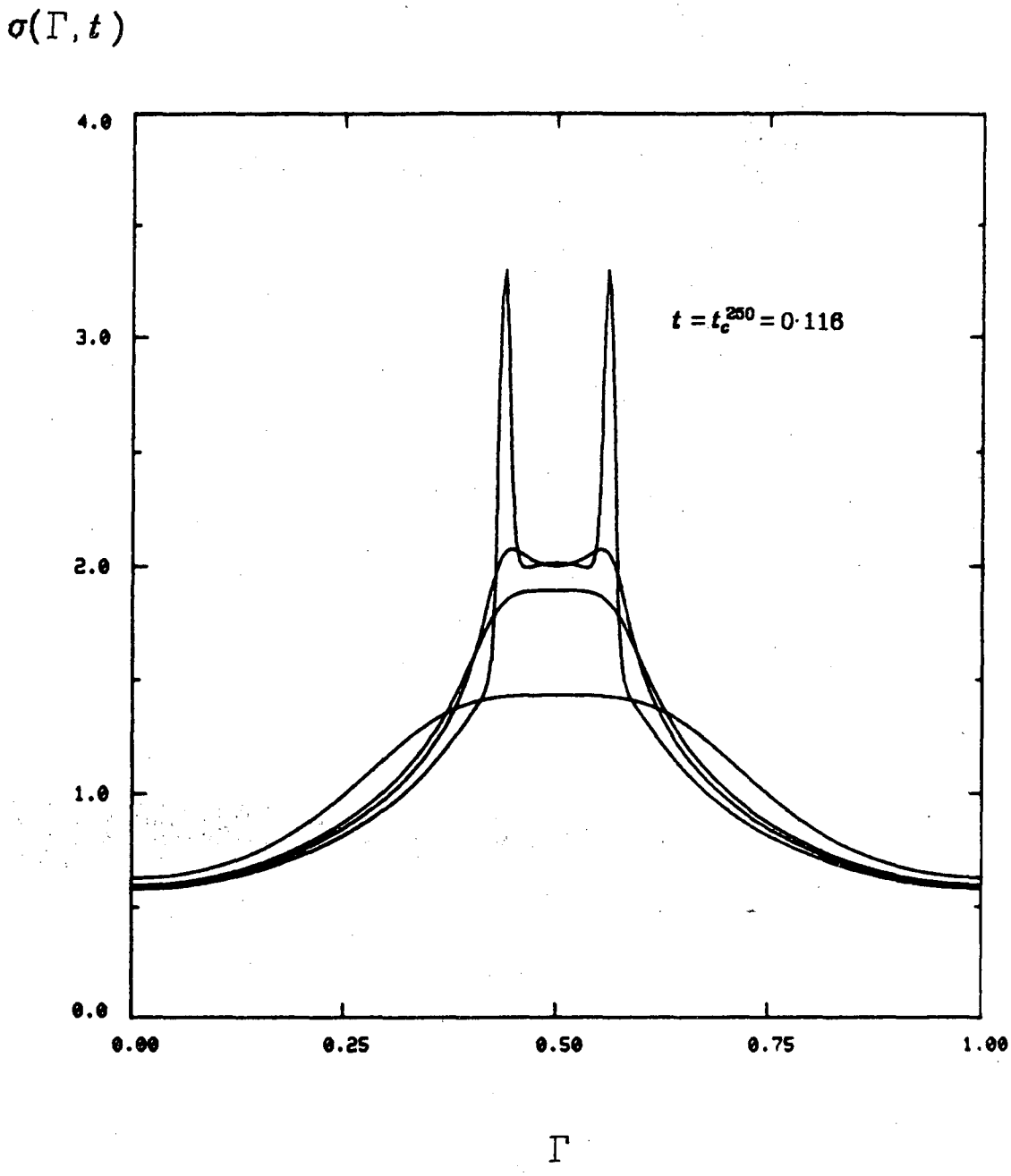

Figure 4.2 A plot of the vortex sheet strength of figure 4.1, vs. Γ for various times. ($t = 0$, $0{\cdot}08$, $0{\cdot}96$, $0{\cdot}116 = t_c^{250}$)

$\ln \hat{P}_{250}|(k,t)|$

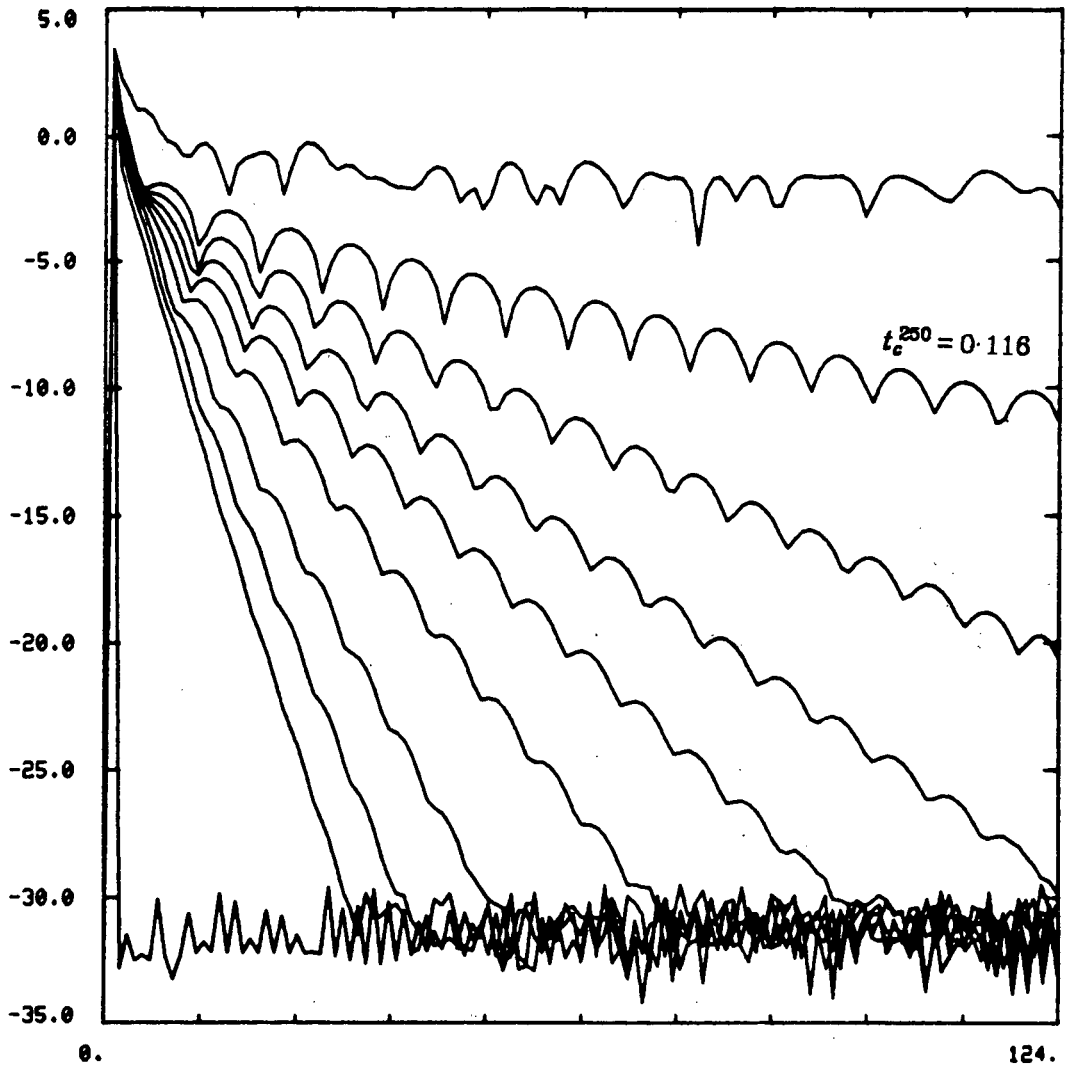

Figure 4.3 A linear-log plot of the spectral amplitudes for figure 4.1 at various times. ($t = 0, 0{\cdot}02, 0{\cdot}04, 0{\cdot}06, 0{\cdot}08, 0{\cdot}092, 0{\cdot}1, 0{\cdot}108, 0{\cdot}116, 0{\cdot}44$)

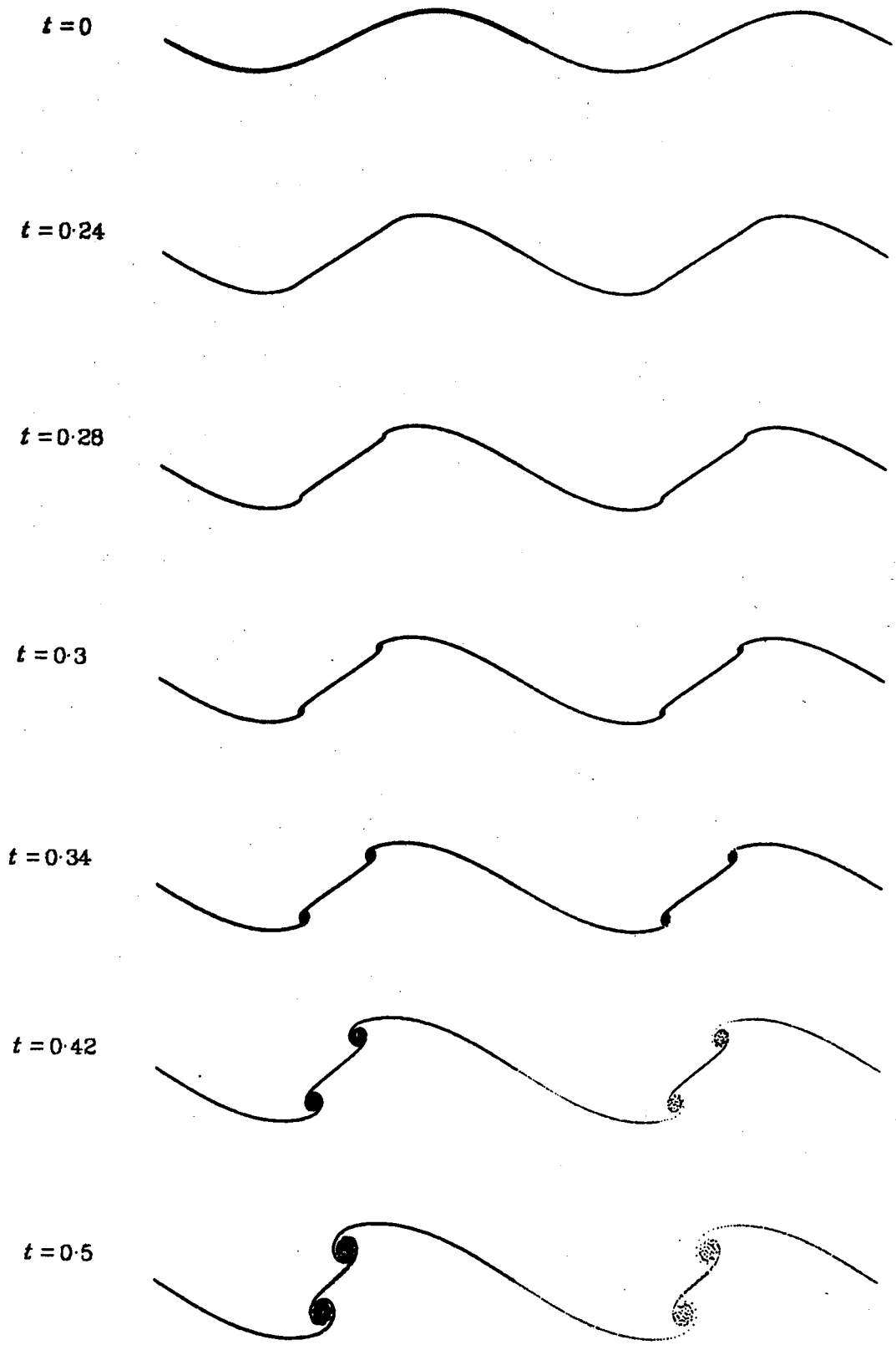

Figure 4.4 Initial condition (4.2) with $\alpha = 0{\cdot}08$.

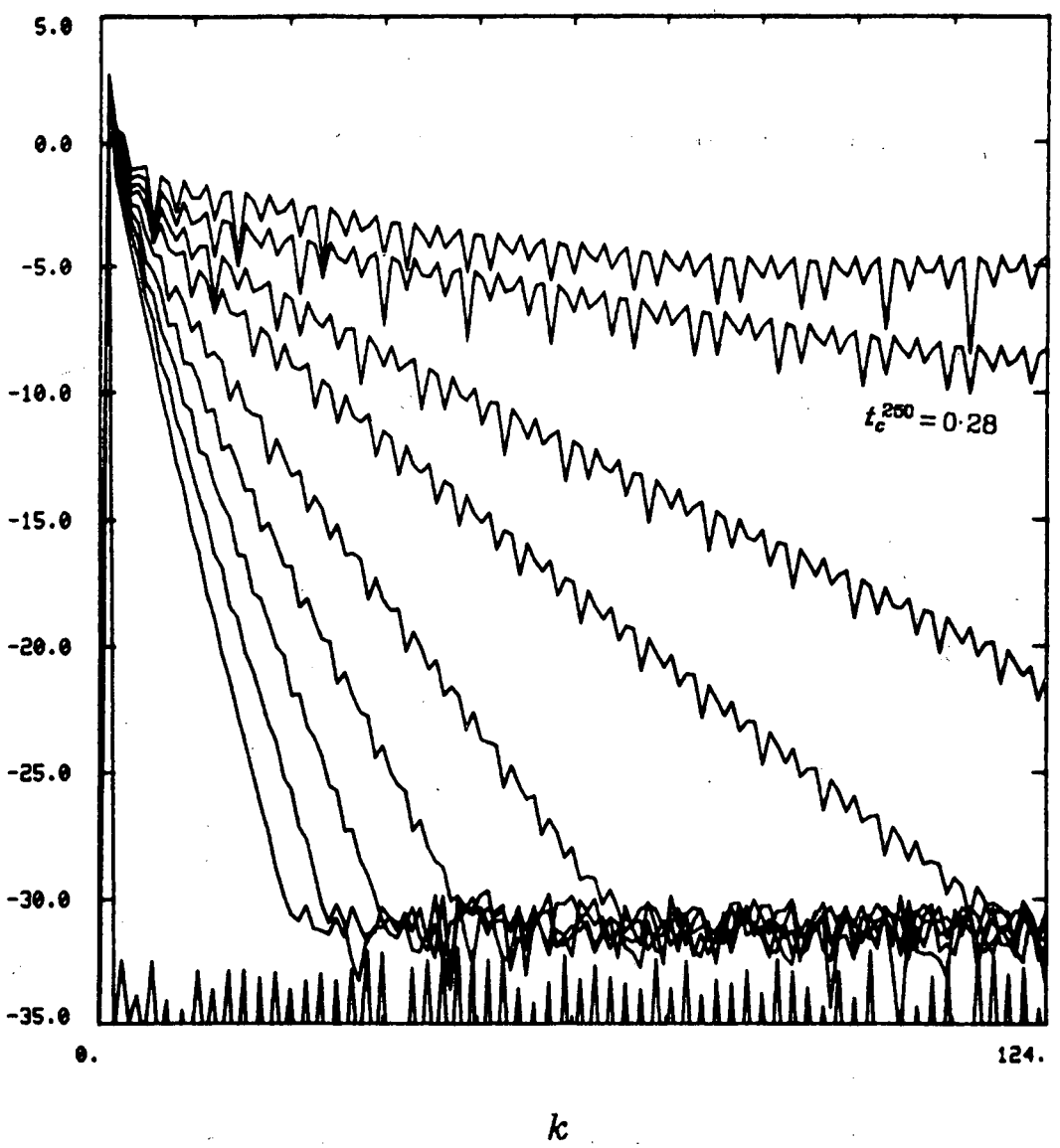

Figure 4.5 A linear-log plot of the spectral amplitudes for figure 4.1 at various times. ($t = 0$, $0{\cdot}04$, $0{\cdot}08$, $0{\cdot}12$, $0{\cdot}16$, $0{\cdot}2$, $0{\cdot}24$, $0{\cdot}26$, $0{\cdot}28 = t_c^{250}$, $0{\cdot}30$)

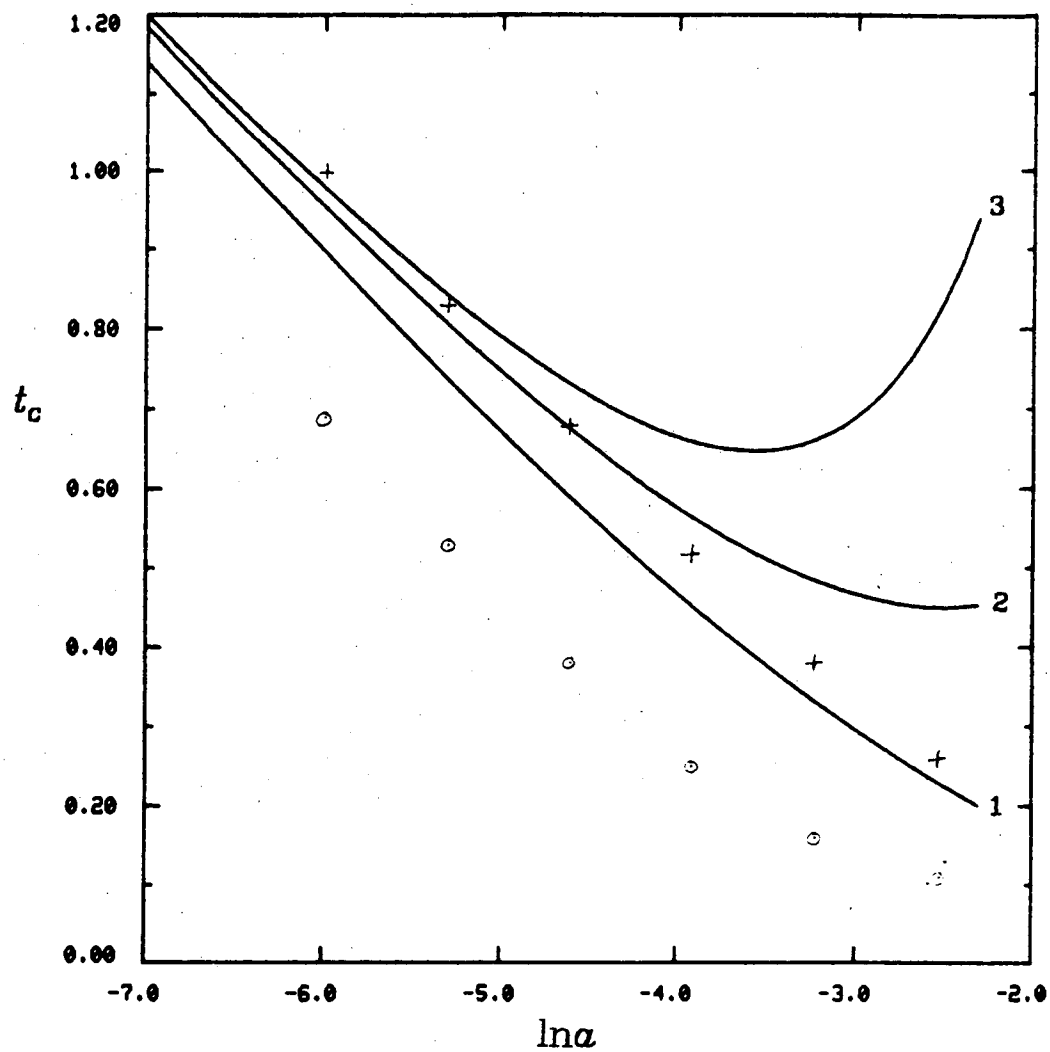

Figure 4.6 The relation between critical time and initial amplitude. The curves show the first three approximations (labelled 1, 2 and 3) given by Moore's asymptotic relation (4.4). Our computed results are plotted for various values of lnα for initial condition (4.1) (0) and for initial condition (4.2) (+). The computed times were obtained by extrapolation to $N \to \infty$ as in Table 4.1 .

Bibliography

Acton, E. 1976 The modelling of large eddies in a two-dimensional shear layer. *J. Fluid Mech.* **76**, 561-592.

Anderson, C. R. 1983 Vortex methods for flows of variable density. *Ph.D. Thesis, University of California, Berkeley*

Ashurst, W. T. 1979 Numerical simulation of turbulent mixing layers via vortex dynamics. In *Turbulent Shear Flows I* Springer-Verlag 402-412.

Baker, G. R. 1980 A test of the method of Fink and Soh for following vortex sheet motion. *J. Fluid Mech.* **100**, 209-220.

Baker, G. R., Meiron, D. I. & Orszag, S. A. 1980 Vortex simulations of the Rayleigh-Taylor instability. *Phys. Fluids* **23**, 1485.

Batchelor, G. K. 1967 *An Introduction to Fluid Mechanics.* Cambridge University Press

Beale, J. T. & Majda, A. 1982 Vortex methods. II: Higher order accuracy in two and three dimensions. *Math. Comp.* **39**, 29-52.

Beale, J. T. & Majda, A. 1983 High order accurate vortex methods with explicit velocity kernels. submitted to *J. Comp. Phys.*

Birkhoff, G. & Fisher, J. 1959 Do vortex sheets roll up? *Rend. Circ. Mat. Palermo ser. 2* **8**, 77-90.

Birkhoff, G. 1962 Helmholtz and Taylor instability. *Proc. Symp. Appl. Math. XIII A.M.S.* 55-76.

Brachet, M. E., Meiron, D. I., Orszag, S. A., Nickel, B., Morf, R. & Frisch, U. 1983 Small-scale structure of the Taylor-Green vortex. *J. Fluid Mech.* **130**, 411-452.

Bromilow, I. G. & Clements, R. R. 1983 A discrete vortex simulation of Kelvin-Helmholtz instability. *AIAA J.* **21**, 1345-1347.

Carrier, G. F., Krook, M. & Pearson, C. E. 1966 *Functions of a Complex Variable*. McGraw Hill 255.

Chandrasekhar, S. 1961 *Hydrodynamic and Hydromagnetic Stabilitity*. Oxford.

Chorin, A. J. 1973 Numerical study of slightly viscous flow. *J. Fluid Mech.* **57**, 785-796.

Chorin, A. J. & Bernard, P. S. 1973 Discretization of a vortex sheet, with an example of roll-up. *J. Comp. Phys.* **13**, 423-429.

Chorin, A. J. 1980 Vortex models and boundary layer instability. *SIAM J. Sci. Stat. Comput.* 1, 1-21.

Chorin, A. J. 1983 The instability of fronts in a porous medium. *Comm. Math. Phys.* **91**, 103-116.

Conte, R. & Sherman, F. S. 1979 Etude numerique des nappes tourbillonnaires

Corcos, G. M. & Sherman, F. S. 1984 The mixing layer: deterministic models of a turbulent flow. Part I - Introduction and the two-dimensional flow. to appear in *J. Fluid Mech.*

Dahlquist, G. & Björck, Å. 1974 *Numerical Methods*. Prentice-Hall. 49.

Fink, P. T. & Soh, W. K. 1978 A new approach to roll-up calculations of vortex sheets. *Proc. Roy. Soc. Lond. A* **362**, 195-209.

Ghoniem, A. F., Chorin, A. J. & Oppenheim, A. K. 1981 Numerical modelling of turbulent flow in a combustion tunnel. *Philos. Trans. Roy. Soc. Lond. A* 1103-1119.

Hald, O. H. 1979 The convergence of vortex methods. II. *SIAM J. Numer. Anal.* **16**, 726.

IMSL Library, Edition 9 1982

International Mathematical & Statistical Libraries, Inc., Houston, Texas.

Kellogg, O. D. 1953 *Foundations of Potential Theory*. Dover. Foundations of potential theory.

Lamb, H. 1932 *Hydrodynamics*. Cambridge University Press

Lax, P. D. 1973 Hyperbolic systems of conservation laws and the mathematical theory of shock waves. *Reg. Conf. Ser. Appl. Math. SIAM* 11.

Longuet-Higgins, M. S. & Cokelet, E. L. 1976 The deformation of steep surface waves on water I. A numerical method of computation. *Proc. Roy. Soc. Lond. A* **350**, 1-26.

Moore, D. W. 1976 The stability of an evolving two-dimensional vortex sheet. *Matematika* **23**, 35-44.

Moore, D. W. 1979 The spontaneous appearance of a singularity in the shape

of an evolving vortex sheet. *Proc. R. Soc. Lond. A* **365**, 105-119.

Moore, D. W. 1981 On the point vortex method. *SIAM J. Sci. Stat. Comput.* **2**, 65-84.

Nakamura, Y., Leonard, A. & Spalart, P. 1982 Vortex simulations of an inviscid shear layer. *AIAA/ASME 3rd Joint Thermophysics, Fluids, Plasma and Heat Transfer Conference* **AIAA-82-0948**

Patnaik, P.C., Sherman, F. S. & Corcos, G. M. 1976 A numerical simulation of Kelvin-Helmholtz waves of finite amplitude. *J. Fluid Mech.* **73**, 215-240.

Pullin, D. I. & Phillips, W. R. C. 1981 On a generalization of Kaden's problem. *J. Fluid Mech.* **104**, 45-53.

Pullin, D. I. 1982 Numerical studies of surface-tension effects in nonlinear Kelvin-Helmholtz and Rayleigh-Taylor instability. *J. Fluid Mech.* **119**, 507-532.

Prandtl, L. & Tietjens, O. G. 1934 *Fundamentals of Hydro- and Aeromechanics*. McGraw-Hill. 222.

Rosenhead, L. 1931 The formation of vortices from a surface of discontinuity. *Proc. R. Soc. Lond. A* A**134**, 170-192.

Saffman, P. G. & Baker, G. R. 1979 Vortex interactions. *Ann. Rev. Fluid Mech.* **11**, 95-122.

Sethian, J. A. 1982 An analysis of flame propagation. *Ph.D. thesis, University of California, Berkeley*

Sulem, C., Sulem, P. L., Bardos, C. & Frisch, U. 1981 Finite time analyticity for the two and three dimensional Kelvin-Helmholtz instability. *Comm. Math. Phys.* **80**, 485-516.

Sulem, C., Sulem, P. L. & Frisch, U. 1983 Tracing complex singularities with spectral methods. *J. Comp. Phys.* **50**, 138-160.

Thompson, C. J. 1979 *Mathematical Statistical Mechanics*. Princeton University Press.

Thorpe, S. A. 1971 Experiments on the instability of stratified shear flows. *J. Fluid Mech.* **46**, 289.

Winant, C. D. & Browand, F. K. 1974 Vortex pairing: a mechanism of turbulent mixing-layer growth at moderate Reynolds number. *J. Fluid Mech.* **63**, 237-255.

Van de Vooren, A. I. 1980 A numerical investigation of the rolling up of vortex sheets. *Proc. R. Soc. Lond. A* **373**, 67-91.

TECHNICAL INFORMATION DEPARTMENT
LAWRENCE BERKELEY LABORATORY
UNIVERSITY OF CALIFORNIA
BERKELEY, CALIFORNIA 94720